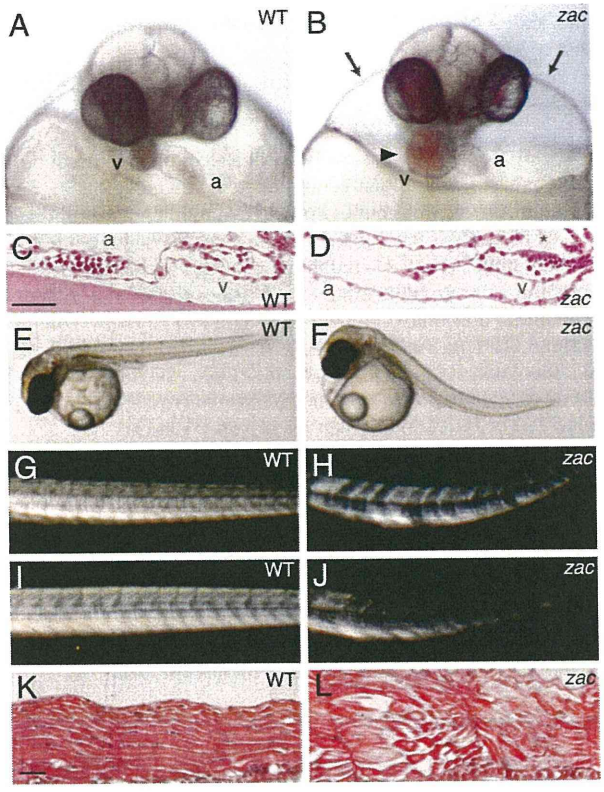

Fig. 1. Cardiac and skeletal muscle phenotypes of *zac* mutants. Embryos from the wild-type (A, C, E, G, I, K) and *zac* mutants (B, D, F, H, J, L). (A, B) Ventricular enlargement in *zac* mutants. Frontal views at stage 28. Dorsal is to the top. Blood cell accumulation in the ventricle (B, arrowhead) and cardiac edema (B, arrows) are visible. a; atrium, v; ventricle (C, D) Hematoxylin and eosin staining of a sagittal section of heart at stage 27. Rostral is to the left. Only the myocardial wall has a rupture (D, asterisk). Scale bar: 20 μm in "C." (E, F) Whole view from the lateral side at stage 32. *zac* mutants show body curvature. (G–J) Birefringence of skeletal muscle at stage 32 (G, H) and stage 34 (I, J). Rostral is to the left. *zac* mutant shows patchy birefringence at stage 32 and overall reduction in birefringence at stage 34. (K, L) Masson trichrome staining of horizontal sections at stage 32. Rostral is to the right. Striated patterns of sarcomeres can be seen in many muscle cells, but some myofibers have severely degenerated in the *zac* mutants. Scale bar in "K": 20 μm.

After hatching, *zac* mutants were not able to swim normally, and they died around 14 days post-fertilization. These phenotypes indicate that the *zac* mutation affected both cardiac and skeletal muscles.

Nonsense mutation in flnc in zac mutants

We performed positional cloning to identify the responsible gene in *zac* mutants. By using sequence-tagged site (STS) markers (Kimura et al., 2004), we mapped the *zac* gene to the marker MF01SSA047D04 on the medaka linkage group 6 (Fig. 2A). We searched the expressed sequence tag (EST) markers around the MF01SSA047D04, and found zero and 2 independent recombinants by using AU171271 and Olb2110h, respectively. Therefore, the *zac* gene was placed in the vicinity of AU171271 between MF01SSA047D04 and Olb2110h (Fig. 2A). We further performed fine mapping by utilizing an additional marker, histidine ammonia-lyase (*HAL*), which gave 1 recombinant and narrowed down the *zac* locus. We also found zero recombinants by using another marker, the potassium voltage-gated channel, Shal-related subfamily, member 2 (*KCND2*). Though the genomic sequence encompassing the *zac* locus contained several open reading frames (ORFs), one of them encoded a protein highly homologous to human filamin C, a cardiac and skeletal muscle-specific isoform of the filamin family.

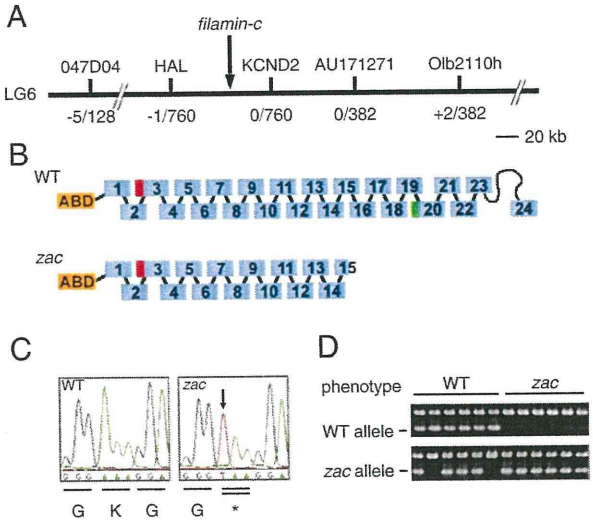

Fig. 2. Positional cloning of *zac* gene (A) Map of the genomic region containing the *zac* gene. The *zac* locus is mapped on the medaka linkage group (LG) 6 by using M-markers, and *flnc* is located in the candidate region. HAL, histidine ammonia-lyase and KCND2, potassium voltage-gated channel, Shal-related subfamily, member 2. Recombination frequencies for the respective markers are shown below. (B) Schematic drawings of filamin C protein in wild-type and *zac* mutant. The actin-binding domain (ABD) is located at N-terminal followed by 24 repeats of filamin domains. The red region between the 2nd and 3rd repeats indicates the unique splicing variation in medaka fish. The green box between the repeats 19th and 20th is a unique sequence in filamin C members. There is only one hinge sequence between the repeat 23rd and 24th in the medaka filamin C. (C) Chromatogram of the cDNA sequence containing a nonsense mutation from A to T in a coding region of *flnc* (arrow). (D) Linkage of *zac* mutation with *flnc* as shown by allele-specific genotyping PCR. WT indicates phenotypically wild-type embryos, so some are genotypically heterozygotes revealing both WT and zac alleles' PCR products and others are genotypically wild-type having WT allele's PCR product only. All *zac* mutants are genotypically homozygotes, which show the zac allele's PCR products only.

The sequence analysis revealed that the medaka *flnc* had a high degree of homology (approximately 77% amino acid identity) to the human *FLNC* (Supplementary Fig. 1). The overall structure of medaka filamin C consisted of the actin-binding domain (ABD) and 24 immunoglobulin-like repeats with a hinge region between the 23rd and the 24th repeats (Fig. 2B). Although there was no spacer region between the 15th and the 16th repeats, as found in chicken *Flnc/cgABP260* (Ohashi et al., 2005) and in some human *FLNCs* (Supplementary Fig. 1), the medaka *flnc* had a C-isotype-specific insertion sequence between the 19th and the 20th repeats (green box in Fig. 2B; blue underline in Supplementary Fig. 1), which is also seen in mouse *Flnc* (Dalkilic et al., 2006). We also found a novel splicing variation of an additional 39 amino acids between the 2nd and 3rd repeats (red box in Fig. 2B).

We sequenced the entire coding sequence of medaka *flnc* from the *zac* mutant and the wild-type sibling alleles and found that the *zac* mutant had a nucleotide substitution from A to T at the first base of codon 1680 (Fig. 2C; AAA to TAA). As a result, this mutation changed the lysine residue to a stop codon (K1680X), causing premature termination in the 15th immunoglobulin-like repeat. This mutation was detected with 100% identity by PCR using allele-specific primers (Fig. 2D).

In the medaka genome database from Ensembl, there is one more filamin C ortholog, which is notated as FLNC (2 of 2). This predicted gene is located mostly in the ultracontig278 and partially in the scaffold698_contig104802. To find the possibility of functional contribution, we examined the sequence similarity of this gene compared to the human filamin C and the medaka filamin C investigated in this study (Supplementary Fig. 2). FLNC (2 of 2) is described as "ol filamin c #3" in this figure. The FLNC (2 of 2) contains 16 filamin-repeats from 9th to 24th repeat of the regular filamin C, and has one hinge region between 23rd and 24th repeat. About three fourth of filamin C-specific region (UR) is pulled out and N-terminal domains of the

actin binding domain and 1–8th repeats are missing. Although the entire sequence is well conserved and the feature of having single hinge represents filamin C, the lack of N-terminal domains is critical. This gene might be termed as "ol flnc 9–24" (Stossel et al., 2001) and functional redundancy would not be expected as for filamin C.

mRNA expression of flnc is markedly reduced in zac mutants

The pattern of *flnc* expression was analyzed by whole-mount RNA *in situ* hybridization. *flnc* expression was first evident in somites and at the rostral tip of notochord at the onset of somitogenesis. Subsequently, by the 6-somite stage, the expression of *flnc* was detected in the cardiac precursor cells in the anterior lateral-plate mesoderm (Fig. 3A). After migration of the myocardial precursor cells towards the midline, the expression of *flnc* was detected in both the atrium and ventricle (Fig. 3C). These expressions of *flnc* in the somites, the rostral tip of the notochord, and the cardiac muscles continued in subsequent stages (Fig. 3E). At later stages, additional expression was seen in the muscles of the pectoral fin joint and head (data not shown). Although the pattern of expression of *flnc* did not differ between the wild-type and *zac* mutants, the level of expression was reduced in the latter (Figs. 3B, D, F).

To further identify whether this lower expression of *flnc* in *zac* mutants was caused by the transcriptional down-regulation or not, we generated a transgenic medaka line expressing EGFP under the regulation of a 3 kb-*flnc* promoter. Both in the wild-type and *zac* mutants, the EGFP transgene was expressed at a similar level (Figs. 3G, H), demonstrating that the transcription of the *flnc* gene was not affected by the *zac* mutation. Moreover, the reduced mRNA expression of *flnc* in *zac* mutants was detected before the appearance of abnormal cardiac and muscular phenotypes (Figs. 3A, B), suggesting that the reduction was not caused by any morphological effect in the *zac* mutants. Taken together, these results suggest that the apparently lower expression of *flnc* in *zac* mutants may have been due to the instability of the mutated mRNAs, as often observed in other cases (Baker and Parker, 2004).

To confirm whether the defect in *flnc* was sufficient to cause the *zac* phenotype, we used morpholino antisense oligonucleotides (MO) targeting the translation of *flnc*. When the MO was injected at a dose of 400 μM, 13% of the injected embryos displayed a *zac*-like cardiac phenotype including the myocardial ruptures (n=94; Figs. 3I, J). In contrast to the heart phenotype, we did not observe an abnormal phenotype in the skeletal muscles of the MO-injected embryos. It appears that the MO may have required a longer time before producing the skeletal muscle phenotype, but the effect of MO might not have been strong enough to affect the skeletal muscles. We tested higher concentrations of MO (500–1000 μM); however, the overall shape of the injected embryos was severely deformed.

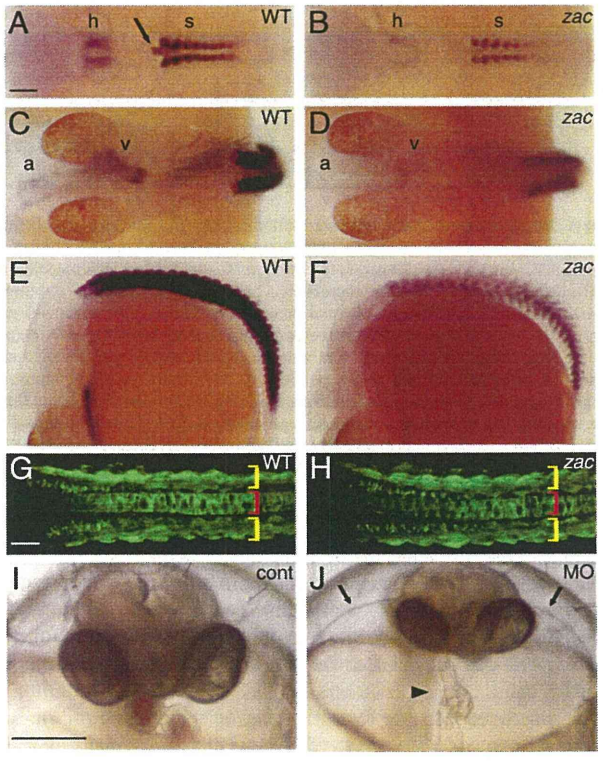

Fig. 3. Expressions of medaka *flnc* in notochord and cardiac and skeletal muscles. Wild-type (A, C, E, G) and *zac* mutant embryos (B, D, F, H). (A–F) Whole-mount RNA *in situ* hybridization analysis of *flnc* expression at stage 22 (A, B) and stage 27 (C–F). Dorsal views (A–D) and lateral views (E, F). Rostral is to the left. *flnc* expression is seen in bilateral cardiac precursor cells (h), somites (s), and the anterior tip of the notochord (arrow). Both atrium (a) and ventricle (v) express *flnc*. Note that *flnc* mRNA expression is reduced in *zac* embryos (B, D, F). (G, H) *flnc* expression visualized in the *flnc* promoter transgenic medaka at stage 26. Dorsal views of the trunk. Rostral is to the left. The level of EGFP expression is not decreased in *zac* mutants, demonstrating that the decrease in the *flnc* mRNAs may be due to instability of mutated *flnc* mRNAs. Yellow and red brackets indicate somites and notochord, respectively. (I, J) Phenocopy by injection of MO. Stage 28, Head frontal views. Dorsal is to the top. Embryos injected with the control MO show the normal appearance (I). However, embryos injected with *flnc*-MO show the cardiac rupture in the ventricle (J: arrowhead) and edema (J: arrows). Scale bars: 100 μm in "A", 50 μm in "G" and 200 μm in "I".

zac mutation affects the maintenance of the muscle structure rather than its formation

Since the expression of *flnc* in medaka embryos was detected in the early stage of development (see Fig. 3), we investigated whether the *zac* mutation affected the differentiation of cardiac or skeletal muscle cells by examining the expression of various differentiation marker genes. The expression patterns and levels of cardiac differentiation markers, such as *nkx 2.5*, *tbx5a*, *des*, *cmlc2*, and *vmhc*, were not changed in *zac* hearts at stage 27 (Figs. 4A, B: *cmlc2*, C, D: *des*, the data for *nkx 2.5*, *tbx5a*, and *vmhc* are not shown). The expressions of muscle differentiation markers such as *myoD*, *myf5*, and *des* were also normal in the trunk and tail up to stage 30 (Figs. 4E–H). These results suggest that the early differentiation of cardiac and skeletal muscle cells was not affected in the *zac* mutants.

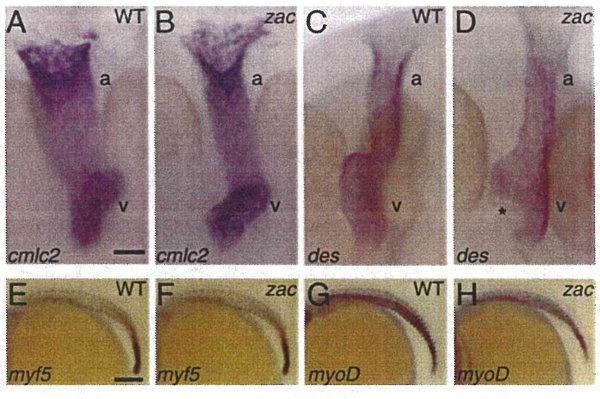

Fig. 4. Expressions of differentiation marker genes in cardiac and skeletal muscle development (A–D). Whole-mount RNA *in situ* hybridization for the expression of cardiomyocyte markers, i.e., *cmlc2* (A, B) and *des* (C, D) at stage 27. Wild-type (A, C) and *zac* mutants (B, D). Dorsal view (A, B) and ventral view (C, D) are shown. Rostral is to the top. Differentiation of cardiomyocytes looks normal. A rupture of the myocardium in the *zac* ventricle is indicated by the asterisk. a; atrium and v; ventricle (E–H) Whole-mount RNA *in situ* hybridization for the expression of muscle markers *myf5* (E, F) and *myoD* (G, H) at stage 27. Wild-type (E, G) and *zac* mutants (F, H). Lateral views. Head is to the left. Both genes show normal expression patterns in the *zac* mutant. Scale bars: 20 μm in "A" and 200 μm in "E".

It has been demonstrated that filamin C protein is localized at the myotendinous junction, Z-disks, and sarcolemma in skeletal muscle fibers, and in the intercalated disks of cardiomyocytes in mammalian and avian hearts (Ohashi et al., 2005; Thompson et al., 2000; van der Ven et al., 2000a). To determine the subcellular localization of filamin C protein in medaka, we performed immunostaining with a filamin C-specific antibody. In the medaka heart, filamin C was localized at cell–cell contact sites between the cardiomyocytes (Fig. 5A). In skeletal muscle, the most abundant expression of filamin C was detected at the junction area where the ends of the muscle fibers attached to the myosepta (Fig. 5B), corresponding to the myotendinous junction (MTJ) in mammals (Summers and Koob, 2002). Filamin C was also localized at the sarcolemma (Figs. 5C–E) and Z-disks (Figs. 5F–H). These results suggest that the localization of filamin C protein is conserved among fish, avians, and mammals.

To examine the effect of filamin C-deficiency on muscle cells, we analyzed *zac* mutants by using a scanning electron microscope (SEM). At stage 27, cardiomyocytes in the *zac* mutant ventricle were not well-ordered ones and had a rougher surface with a number of lamellipodia- and filopodia-like structures (Figs. 6B, D) compared with those in the wild-type heart (Figs. 6A, C), although there was no significant difference in the atrium. These changes were more evident after the onset of blood circulation. Transmission electron microscopic (TEM) analysis of the wild-type heart revealed that organized myofibrils ran along the inner surface side of the cardiomyocytes with the nuclei being located at the outer surface side (Fig. 6E). In contrast, the cytoplasmic structure and subcellular localization of nuclei were severely disorganized in the *zac* mutant (Fig. 6F). Although myofibrils were present even after the rupture of the heart, which is consistent with the fact that the *zac* heart was able to contract, it is also important to note that fewer sarcomere bundles were attached to the intercalated disks in the *zac* mutants (Figs. 6G, H). Large vacuoles, which contained no sarcoplasmic or membranous materials, were observed in *zac* cardiomyocytes (Fig. 6H). The muscle sarcomere is the important structure for establishing cell–cell adhesion at the intercalated disk between the myocardial cells. Our observations suggest that the *zac* mutation may have interfered with the formation and/or maintenance of the sarcomere structures in the myocardium and that weakened cell–cell adhesion might have resulted in the rupture frequently seen in the ventricle, which is supposed to resist high contraction pressure.

Skeletal muscle was also analyzed by TEM. Although *flnc* was expressed from the onset of somitogenesis, the sarcomere structures in the *zac* mutants were normally formed in most of the skeletal muscle fibers and maintained even at stage 30 (Figs. 7A, B). Only in some somites of *zac* mutants had myofibrils degenerated at MTJs at stage 32 (Figs. 7C–F). In addition, focal disorganization of the sarcomere structure was observed in *zac* mutants. In the disorganized area, Z-disks were faint or totally missing (Figs. 7G, H). Many large vacuoles were also observed in *zac* skeletal muscle (Figs. 7I, J). The sarcolemma was frequently detached from the myofibrils, and dilated sarcoplasmic reticula occupied the space between them, in

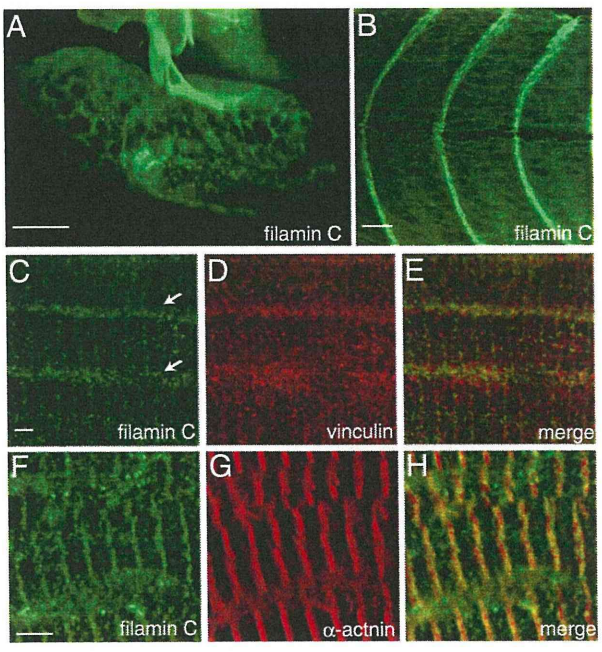

Fig. 5. Subcellular localization of filamin C protein in heart and skeletal muscles. Immunofluorescence staining of filamin C protein in the wild-type embryos. Filamin C is localized at cell–cell contact sites in the heart at stage 32 (A), in the junctional area where the ends of muscle fibers attach to the myosepta (corresponding to myotendinous junction) at stage 32 (B), and in the sarcolemma (C, arrows and merge in "E"), and Z-disks (F and merge in "H") at stage 40. (C–E) Double staining of filamin C (C), vinculin (D), and their merged image (E). (F–H) Double staining of filamin C (F), α-actinin (G), and their merged image (H). (B–H) Rostral is to the left. Lateral view. Scale bar: 20 μm in "A" and "B", 2 μm in "C" and 4 μm in "F".

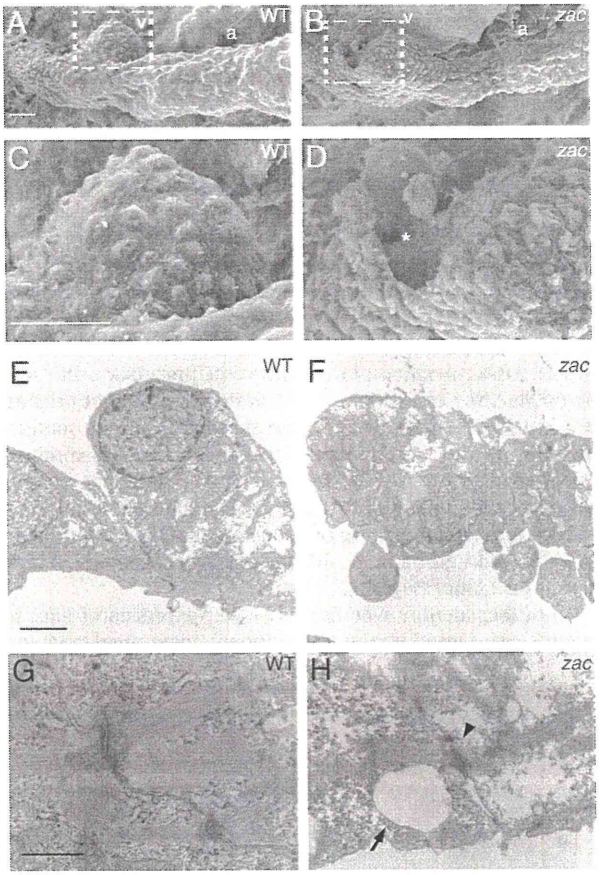

Fig. 6. Ultrastructure of cardiomyocytes. Embryos from the wild-type (A, C, E, G) and *zac* mutants (B, D, F, H). (A–D) Scanning electron microscopic analysis of heart tube at stage 27. Ventral views. Rostral is to the right. "C" and "D" are high magnifications of the boxed area in "A" and "B", respectively. Cardiomyocytes around the rupture (asterisk) in the *zac* heart show a rough and irregular cell surface. a; atrium and v; ventricle. (E–H) Transmission electron microscopic analysis of cardiomyocytes at stage 27. (E, F) Outer surface of the heart tube is to the top. Cardiomyocytes in *zac* mutants show an abnormal subcellular organization. (G, H) Ultrastructure of intercalated disks at stage 29. Fewer sarcomere bundles are connected to the intercalated disks in *zac* mutants (H, arrowhead) compared with their number in the wild-type (G) at stage 29. Large vacuoles are frequently observed in the *zac* mutants (H, arrow). Scale bar: 20 μm in "A", 10 μm in "C", 2 μm in "E" and 1 μm in "G".

the *zac* muscle at stage 36 (Figs. 7K, L). These results suggest that filamin C may have contributed to the stabilization of myofibrils at the MTJ, maintenance of the Z-disk structures, and attachment of myofibrils to sarcolemma rather than be involved in myofibril formation.

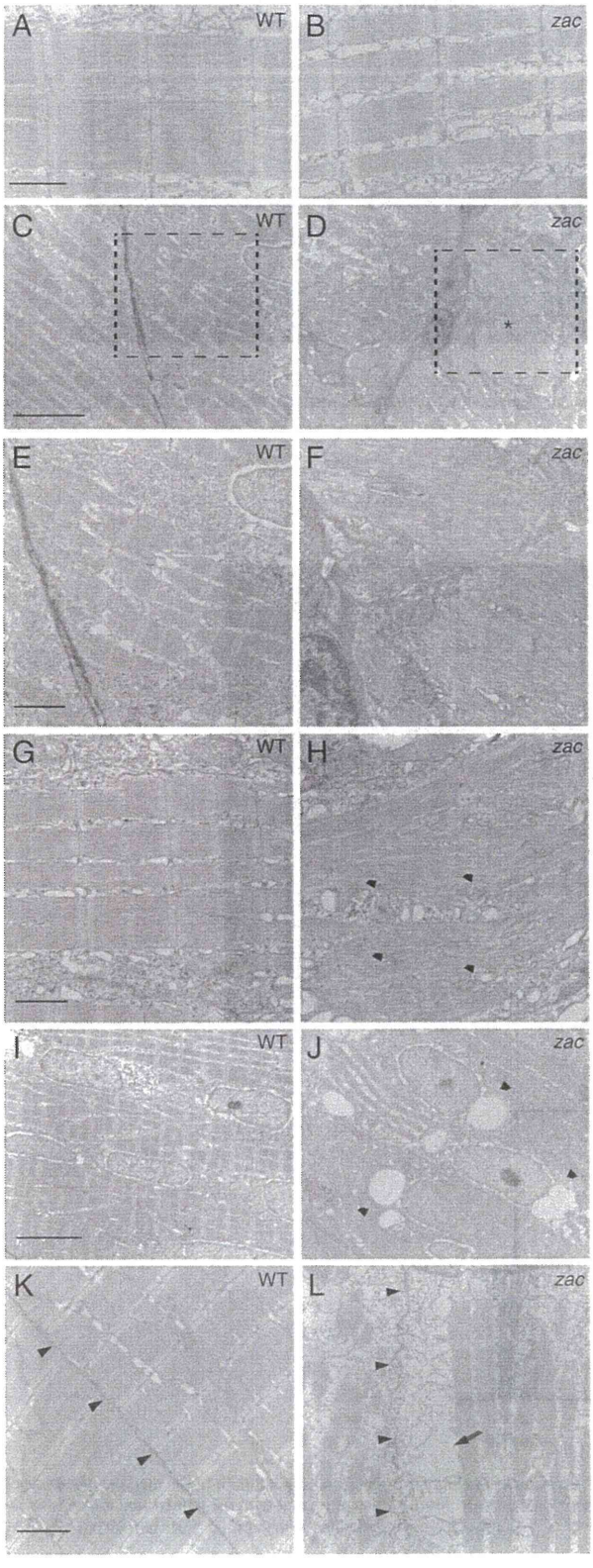

Reduction in amount of γ-actin at MTJs

Filamins crosslink actin filaments, and link them to cellular membrane by binding to the transmembrane proteins (Stossel et al., 2001). Filamin C interacts with β1-integrin (Gontier et al., 2005; Loo et al., 1998) and δ/γ-sarcoglycans (Thompson et al., 2000), the components of the DGC. Both complexes are concentrated at MTJs, and have an important role to link subsarcolemmal γ-actin filaments to the ECM in mammals. Since muscle fibers at the MTJs were affected in *zac* mutants, we evaluated the effect of the *zac* mutation on the localization of the proteins involved in this linkage system. Since we did not find any antibodies crossreactive with medaka δ/γ-sarcoglycans, we assessed the sarcoglycan complex by using antibodies against β-sarcoglycan (β-SG). It is known that the entire sarcoglycan complex, containing α-, β-, γ-, and δ-sarcoglycans, becomes destabilized, resulting in decreased localization at the sarcolemma, when any one of its components is disrupted in mammals or zebrafish (Guyon et al., 2005; Mizuno et al., 1994). Similar to the filamin C, integrin β1D, β-sarcoglycan (β-SG), and γ-actin were accumulated at the MTJ in the wild-type medaka (Fig. 8, upper panels). Although the expressions of integrin β1D and β-sarcoglycan were not altered in the *zac* mutants, γ-actin was markedly reduced at their MTJs (Fig. 8, lower panels). We also analyzed β-dystroglycan and dystrophin (other components of the DGC) and the phosphorylated forms of FAK and paxillin (downstream molecules of integrin signaling). The results revealed that these molecules were also accumulated at MTJs with no obvious difference in signals between the wild-type and *zac* mutants (data not shown). Since the filamin C is also localized at Z-disks (see Figs. 5F–H), we examined whether the filamin C mutation primarily affected the formation of Z-disks. Double immunostaining of γ-actin and α-actinin revealed that at stage 32 when γ-actin was already altered (Supplementary Fig. 3, upper panels), α-actinin-stained Z-disks were detected normally in *zac* myotome muscle (Supplementary Fig. 3, lower panels), indicating that the primary consequence of the deficiency of filamin C is the defect in the linkage system, not in the Z-disk. These results suggest that filamin C functions to maintain the structural integrity at the MTJs via γ-actin.

zac mutant is more susceptible to mechanical stress by muscle contraction

The observations by electron microscopy and immunohistochemistry demonstrated that muscle degeneration occurred not equally but stochastically in the *zac* mutants. In addition, muscle damage was frequently observed at MTJs, where myofibrils are exposed to strong mechanical stress from muscle contraction. These observations led us to investigate whether muscle degeneration was related to muscle contraction. So we incubated medaka embryos in a solution of tricaine methanesulfonate, which is a common reagent for anesthetizing fish by blocking the action potential. We found that a 0.0015% solution of tricaine methanesulfonate could suppress muscle contraction in medaka embryos without blocking heart beats at stage 27. Under this condition, all embryos survived from stages 27 to 32. So we incubated embryos in this anesthetic and evaluated muscle

Fig. 7. Ultrastructure of longitudinal section of skeletal muscle. Embryos of wild-type (A, C, E, G, I, K) and *zac* mutant (B, D, F, H, J, L). (A, B) Sarcomere structures are normally formed in *zac* mutants at stage 30. (C–F) Myofibrils have degenerated at myotendinous junctions (asterisk) at stage 32. "E" and "F" are high magnifications of the boxed area in "C" and "D", respectively. (G, H) Focal disorganization of the sarcomere structure at stage 32. Z-disks are not observed in some myofibrils in *zac* mutants (H, arrowheads). (I, J) Large vacuoles (J, arrowheads) are frequently observed in *zac* mutants at stage 32. They are single-membrane vacuoles, and no sarcomeric or membranous material is seen inside. (K, L) Detachment of sarcolemma from myofibrils in *zac* mutants at stage 36. Even though sarcomere structures are well-preserved, the sarcolemma (arrowheads) has become detached, and dilated sarcoplasmic reticula (L, arrow) occupy the space in *zac* mutants. Scale bar: 1 μm in "A" and "G", 5 μm in "C" and "I" and 2 μm in "E" and "K".

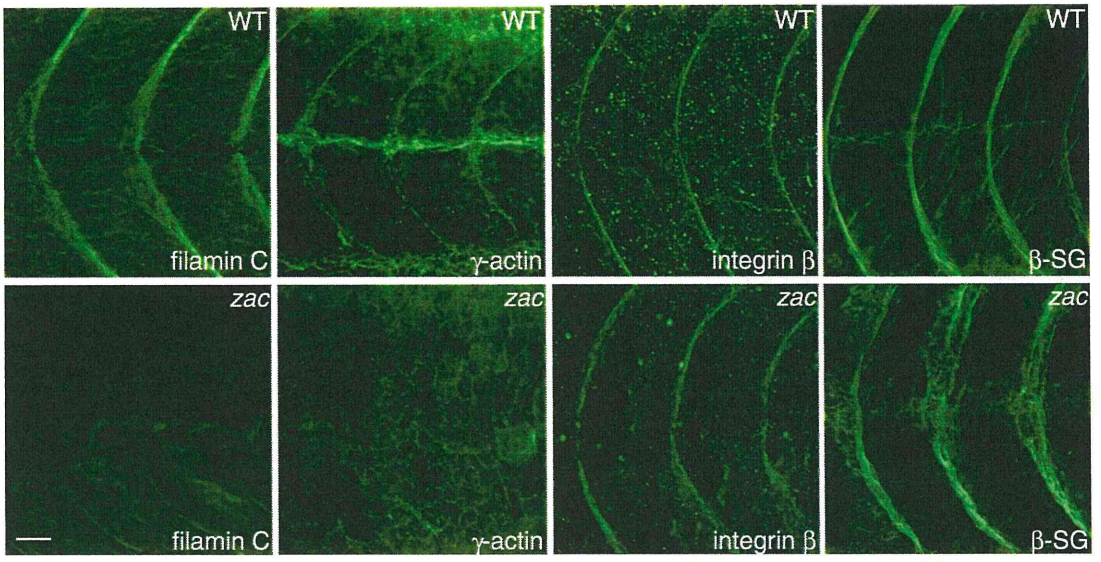

Fig. 8. Immunofluorescence analysis of MTJ. Immunofluorescence stainings of filamin C, γ-actin, integrin β1D and β-sarcoglycan (β-SG). Each of these proteins accumulates prominently at the MTJ in the wild-type. Only γ-actin protein expression is reduced in the *zac* mutants, whereas other proteins are retained. Rostral is to the left. Stage 32. Scale bar: 20 μm.

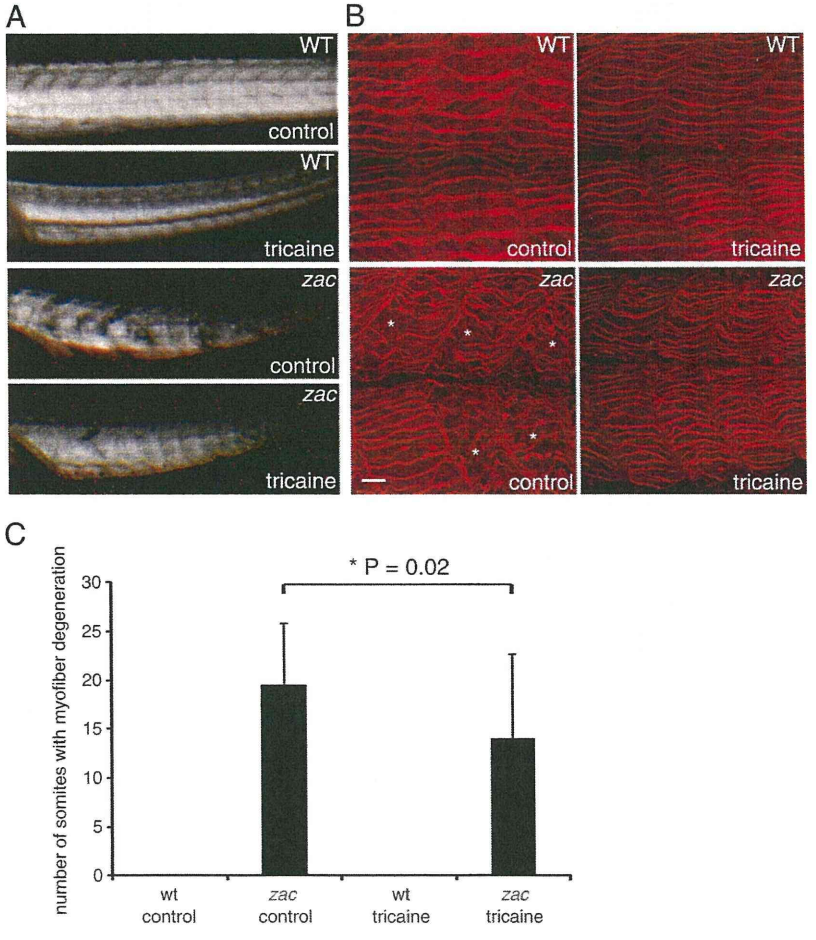

Fig. 9. *zac* mutant is more susceptible to mechanical stress by muscle contraction. (A) Birefringence assay of embryos in the control medium or in the medium containing the anesthetic tricaine methanesulfonate (tricaine). The anesthetized *zac* mutant shows a milder reduction in muscle birefringence compared with the non-treated *zac* mutant. (B) Slow muscle myosin heavy chain staining (F59) of control and anesthetized fish at stage 32. Asterisks show somites having muscle fiber degeneration. Scale bar: 20 μm. (C) Quantification of muscle degeneration. N = 20. P = 0.02.

degeneration. Anesthetized wild-type embryos appeared to be a bit smaller and skinnier compared with non-treated wild-type embryos, but did not show any perturbed birefringence. As expected, inhibition of locomotion restored muscle birefringence in the *zac* mutants (Fig. 9A). This finding was further confirmed by immunostaining of the slow muscle myosin heavy chain, which staining revealed a decreased level of myofiber disorganization in the anesthetized *zac* mutants (Figs. 9B, C). The myofibers in anesthetized wild-type embryos were thinner than those in the non-treated wild-type embryos, but never had degenerated or become disorganized. Loss of accumulation of γ-actin at the MTJs was not recovered under the tricaine treated condition in the *zac* mutants (data not shown), suggesting that the defect of γ-actin is not contraction-dependent. This is rather supporting the idea that γ-actin is linked to the MTJs by filamin C to reinforce the muscle structure. These results suggest the protective role of filamin C against the mechanical stress to myofibrils caused by muscle contraction.

Discussion

Function of filamin C in the heart

Mutations in human *FLNC* cause a myopathy with altered myofibril organization (Kley et al., 2007; Luan et al., 2010; Shatunov et al., 2009; Vorgerd et al., 2005). These patients frequently show a cardiomyopathy, but the mechanisms causing the cardiac symptom elicited by the each mutation in filamin C have remained unclear. We found that the loss of filamin C in medaka led to cardiac rupture in the ventricular myocardium. Unlike other fish mutants of muscle sarcomere proteins, for example, *pik/ttna* and *sih/tnnt2* (Sehnert et al., 2002; Xu et al., 2002), in which heart beating is severely damaged, the *zac* mutant heart started beating normally, and this beating continued. On the other hand, once the heart beating started, a limited region of the ventricle ruptured, though *flnc* was expressed in all myocardial cells. One reason for this tendency for a limited rupture region is that the ventricle was exposed to higher mechanical stress caused by contraction than was the atrium. Thus, this *zac* mutant phenotype indicates that the loss of filamin C may have weakened the mechanical strength of the heart. In accordance with this notion, we observed that the *zac* cardiomyocytes had an abnormally ruffled cell membrane surface, which is probably a consequence of failure of proper cell–cell adhesion, as previously described in the case of *in vitro* cultured cells (Borm et al., 2005). Moreover, TEM analysis revealed that fewer sarcomere bundles were attached to the intercalated disks, where the muscle sarcomeres are involved in establishing cell–cell adhesion. Based on all of our data taken together, we propose that the function of filamin C in the heart may be required for the integrity and stability of the cardiomyocytes.

Compared with the medaka *zac* mutant, the heart phenotype has not been highlighted in the mouse filamin C-deficient model (Dalkilic et al., 2006). This mouse is designed to generate a partial-loss-of-function model, which lacks only the repeats 20th–24th. The expression of a truncated filamin C was detected in this mouse model, especially at a higher level in heart than in skeletal muscle. Similar truncation mutations in *FLNA* have caused total- or partial-loss-of-function phenotypes in human patients (Feng and Walsh, 2004). Like *FLNA* and *FLNB* mutations (Krakow et al., 2004; Robertson et al., 2003), the position of the mutation may be responsible for variation in the phenotypes in *FLNC*. Recently, Duff et al. reported that mutations in the actin-binding domain of filamin C cause a distal myopathy, in which muscle pathology is totally different from the previous cases having myofibrillar myopathy, which is caused by mutations in either the rod or the dimerization domain of filamin C (Duff et al., 2011). In *zac* mutants, a nonsense mutation in the 15th repeat caused a marked reduction in the level of *flnc* mRNA, such that it was barely detectable in the heart (see Fig. 3F). In addition, translational knockdown by injecting MO revealed a cardiac phenotype similar to that of the *zac* mutant. Taken together, our present findings indicate that the *zac* mutation may represent complete disruption of the filamin C function, leading to severer phenotypes than those seen in the mouse model.

Function of filamin C in skeletal muscle

Since the expression of filamin C started at the onset of somitogenesis, we examined the effect of the *zac* mutation on muscle differentiation. The expressions of muscle differentiation markers were normal, and most of the muscle fibers showed a completely normal structure, based on the electron microscopic observations made at the early stage. However, muscle degeneration started in focal areas, and progressed, with the result being that a larger area became affected by the hatching stage. This progressive muscle phenotype reminded us of its similarity to the one in filamin C-deficient mice, where most fibers exhibited a normal sarcomeric structure, and only some fibers showed Z-disk abnormality. These results suggest that filamin C plays a role in the maintenance of the muscle structure rather than one in myofibrillogenesis in medaka as well as in mammals.

We observed the accumulation of γ-actin at MTJs in wild-type medaka embryos (see Fig. 8). In mammalian muscle fibers, γ-actin exclusively constitutes the subsarcolemmal actin-based cytoskeleton (Rybakova et al., 2000). The γ-actin filaments provide a structural support to muscle fibers by interacting with DGC and the integrin complex. In medaka embryos, DGC and integrin as well as filamin C were concentrated at the MTJs (Fig. 8). Filamin C interacts with both DGC and integrin (Gontier et al., 2005; Loo et al., 1998; Thompson et al., 2000). It was reported that filamin A, the homologue of filamin C, protects cells from mechanical stress by increasing the rigidity of the cortical actin cytoskeleton in non-muscle cells (D'Addario et al., 2001; D'Addario et al., 2003; Shifrin et al., 2009). Thus, it is most likely that filamin C is involved in the linkage system through its interaction with the actin cytoskeleton, DGC, and integrin at the MTJs. Actually, the γ-actin content was reduced and myofibrils were severely affected at the MTJ in *zac* mutants (Figs. 7D, F and 8). Moreover, sarcomere structures in zac mutants were more fragile to mechanical stress caused by muscle contraction (Fig. 9). From these results, we suggest that filamin C participates in the linkage system at the MTJs through the stabilization of γ-actin filaments, protecting sarcomere structures from mechanical stress. In addition, γ-actin is also localized at Z-disks (Nakata et al., 2001), as was filamin C observed presently. Our TEM observation revealed that Z-disks were absent in some myofibrils in the *zac* mutants in late stages and that the sarcolemma had detached from the myofibrils, suggesting another role for filamin C in the lateral connections between myofibrils or between myofibrils and the sarcolemma. Unlike the skeletal muscle, cardiac muscle did not show expression of γ-actin in medaka (data not shown), which is consistent with that γ-actin is expressed mainly in smooth muscle actin (Herman, 1993). Different mechanism and interacting partners with filamin C might be involved to retain the mechanical stability at the intercalated disk in cardiomyocytes.

Patients with mutations in either the rod or the dimerization domain of filamin C show large protein aggregates containing the filamin C itself and its interacting proteins, myotilin and Xin, as well as Z-disk-associated proteins, desmin and αB-crystallin, in the cytoplasm of their muscle fibers (Kley et al., 2007; Luan et al., 2010; Shatunov et al., 2009). Ectopic expression of DGC components in the cytoplasm is also observed. Also, it was demonstrated that the W2710X mutation disturbs the structural stability of filamin C protein, leading to perturbed dimerization (Lowe et al., 2007). As a consequence, it has been suggested that mutant filamin C becomes prone to form aggregates, recruiting its interacting proteins into these aggregates. On the other hand, we did not observe any protein aggregates or cytoplasmic expressions of DGC components in the *zac* mutant. Since the expression of mutant filamin C was remarkably decreased in *zac* mutants, it may have not affected the

localization of the interacting proteins. Instead of aggregates, large vacuoles and dilated sarcoplasmic reticulum were observed electron microscopically in cardiac and skeletal muscle fibers in the *zac* mutants (see Figs. 6H and 7J). These vacuoles, which consisted of a single membrane, did not contain any sarcomeric or membranous materials. These features are totally different from the rimmed vacuoles often seen in patients with the W2710X mutation. Non-rimmed vacuoles with strong PAS-positivity were also reported in these patients, but no accumulation of glycogen was seen in the vacuoles in the *zac* mutants. These vacuoles were not described in the mouse model of filamin C-deficiency, either. Although the presence of vacuoles and dilated sarcoplasmic reticula were described in a report on mechanically induced cell death (Kainulainen et al., 2002) or on animal models of collagen VI-deficiency myopathy, in which apoptosis is enhanced in the skeletal muscle (Irwin et al., 2003; Telfer et al., 2010), the level of apoptosis, as assessed by the TUNEL assay, was not altered in the *zac* mutants (data not shown). Furthermore, no nuclei showing features of apoptosis, such as chromatin condensation, were observed in them. Further studies are required to explain the mechanism of vacuole formation and sarcoplasmic reticulum dilatation.

In light of all of our data taken together, we propose a working hypothesis in which filamin C plays an essential role in maintaining the skeletal and cardiac muscle cell alignment and structure, which hypothesis would explain how these muscles can resist mechanical forces to retain the integrity and stability of their adhesion machineries. Filaminopathy patients frequently develop cardiomyopathy, but the cellular basis for the occurrence of these symptoms has been obscure. Therefore, our analysis using the medaka *zac* mutant offers a useful animal model for understanding the function of filamin C in the maintenance of the structural integrity of muscle cells. Moreover, it has not been proved yet that the function of filamin C is linked to the severe heart phenotype such as the rupture of heart chambers seen in humans. It is possible that filamin C may be associated with idiopathic cardiomyopathy. Further functional analyses may provide us a better understanding of the molecular mechanism of filamin C by which muscular tissues are maintained against mechanical stress.

Finally, regarding the medaka filamin C ortholog: FLNC (2 of 2), to find whether it is involved in Filamin C function in medaka, the further development of medaka genome research is required to confirm the whole genome structure of FLNC (2 of 2).

Supplementary materials related to this article can be found online at doi:10.1016/j.ydbio.2011.10.008.

Acknowledgments

We thank Y. Ishikawa (National Institute for Radiological Sciences, Japan) and members of the screening team for isolating mutants. We thank Y. Takahashi (Iwate Medical University) for heart sectioning and hematoxylin/eosin Y staining, as well as K. Inohaya and Y. Nakatani for their helpful support and discussions. We thank H. Yorifuji (Gunma University Graduate School of Medicine) for providing anti-γ-actin antibody. Hatching enzyme was obtained from National BioResource Project Medaka, Japan. This study was supported by the following sources: a grant-in-aid for scientific research from Japan Society for the Promotion of Science and grants from the programs Research on Psychiatric and Neurological Diseases and Mental Health; Research on Measures for Intractable Diseases; Health Labour Sciences Research Grants for Nervous and Mental Disorders (20B-12, 20B-13) from the Ministry of Health, Labor, and Welfare; and Intramural Research Grants (23-4, 23-5, 23-6) for Neurological and Psychiatric Disorders of NCNP.

References

Anastasi, G., Cutroneo, G., Gaeta, R., Di Mauro, D., Arco, A., Consolo, A., Santoro, G., Trimarchi, F., Favaloro, A., 2009. Dystrophin–glycoprotein complex and vinculin–talin–integrin system in human adult cardiac muscle. Int. J. Mol. Med. 23, 149–159.

Arahata, K., Ishiura, S., Ishiguro, T., Tsukahara, T., Suhara, Y., Eguchi, C., Ishihara, T., Nonaka, I., Ozawa, E., Sugita, H., 1988. Immunostaining of skeletal and cardiac muscle surface membrane with antibody against Duchenne muscular dystrophy peptide. Nature 333, 861–863.

Baker, K.E., Parker, R., 2004. Nonsense-mediated mRNA decay: terminating erroneous gene expression. Curr. Opin. Cell Biol. 16, 293–299.

Bao, Z.Z., Lakonishok, M., Kaufman, S., Horwitz, A.F., 1993. Alpha 7 beta 1 integrin is a component of the myotendinous junction on skeletal muscle. J. Cell Sci. 106, 579–589.

Bassett, D.I., Bryson-Richardson, R.J., Daggett, D.F., Gautier, P., Keenan, D.G., Currie, P.D., 2003. Dystrophin is required for the formation of stable muscle attachments in the zebrafish embryo. Development 130, 5851–5860.

Bonnemann, C.G., Modi, R., Noguchi, S., Mizuno, Y., Yoshida, M., Gussoni, E., McNally, E.M., Duggan, D.J., Angelini, C., Hoffman, E.P., 1995. Beta-sarcoglycan (A3b) mutations cause autosomal recessive muscular dystrophy with loss of the sarcoglycan complex. Nat. Genet. 11, 266–273.

Borm, B., Requardt, R.P., Herzog, V., Kirfel, G., 2005. Membrane ruffles in cell migration: indicators of inefficient lamellipodia adhesion and compartments of actin filament reorganization. Exp. Cell Res. 302, 83–95.

Burkin, D.J., Kaufman, S.J., 1999. The alpha7beta1 integrin in muscle development and disease. Cell Tissue Res. 296, 183–190.

Campbell, K.P., 1995. Three muscular dystrophies: loss of cytoskeleton–extracellular matrix linkage. Cell 80, 675–679.

Cheng, L., Guo, X.F., Yang, X.Y., Chong, M., Cheng, J., Li, G., Gui, Y.H., Lu, D.R., 2006. Delta-sarcoglycan is necessary for early heart and muscle development in zebrafish. Biochem. Biophys. Res. Commun. 344, 1290–1299.

D'Addario, M., Arora, P.D., Ellen, R.P., McCulloch, C.A., 2003. Regulation of tension-induced mechanotranscriptional signals by the microtubule network in fibroblasts. J. Biol. Chem. 278, 53090–53097.

D'Addario, M., Arora, P.D., Fan, J., Ganss, B., Ellen, R.P., McCulloch, C.A., 2001. Cytoprotection against mechanical forces delivered through beta 1 integrins requires induction of filamin A. J. Biol. Chem. 276, 31969–31977.

Dalkilic, I., Schienda, J., Thompson, T.G., Kunkel, L.M., 2006. Loss of filaminC (FLNc) results in severe defects in myogenesis and myotube structure. Mol. Cell. Biol. 26, 6522–6534.

Duff, R.M., Tay, V., Hackman, P., Ravenscroft, G., McLean, C., Kennedy, P., Steinbach, A., Schoffler, W., van der Ven, P.F., Furst, D.O., Song, J., Djinovic-Carugo, K., Penttila, S., Raheem, O., Reardon, K., Malandrini, A., Gambelli, S., Villanova, M., Nowak, K.J., Williams, D.R., Landers, J.E., Brown Jr., R.H., Udd, B., Laing, N.G., 2011. Mutations in the N-terminal actin-binding domain of filamin C cause a distal myopathy. Am. J. Hum. Genet. 88, 729–740.

Ervasti, J.M., 2003. Costameres: the Achilles' heel of Herculean muscle. J. Biol. Chem. 278, 13591–13594.

Faulkner, G., Pallavicini, A., Comelli, A., Salamon, M., Bortoletto, G., Ievolella, C., Trevisan, S., Kojic, S., Dalla Vecchia, F., Laveder, P., Valle, G., Lanfranchi, G., 2000. FATZ, a filamin-, actinin-, and telethonin-binding protein of the Z-disc of skeletal muscle. J. Biol. Chem. 275, 41234–41242.

Feng, Y., Walsh, C.A., 2004. The many faces of filamin: a versatile molecular scaffold for cell motility and signalling. Nat. Cell Biol. 6, 1034–1038.

Gontier, Y., Taivainen, A., Fontao, L., Sonnenberg, A., van der Flier, A., Carpen, O., Faulkner, G., Borradori, L., 2005. The Z-disc proteins myotilin and FATZ-1 interact with each other and are connected to the sarcolemma via muscle-specific filamins. J. Cell Sci. 118, 3739–3749.

Granato, M., van Eeden, F.J., Schach, U., Trowe, T., Brand, M., Furutani-Seiki, M., Haffter, P., Hammerschmidt, M., Heisenberg, C.P., Jiang, Y.J., Kane, D.A., Kelsh, R.N., Mullins, M.C., Odenthal, J., Nusslein-Volhard, C., 1996. Genes controlling and mediating locomotion behavior of the zebrafish embryo and larva. Development 123, 399–413.

Gupta, V., Kawahara, G., Gundry, S.R., Chen, A.T., Lencer, W.I., Zhou, Y., Zon, L.I., Kunkel, L.M., Beggs, A.H., 2011. The zebrafish dag1 mutant: a novel genetic model for dystroglycanopathies. Hum. Mol. Genet. 20, 1712–1725.

Guyon, J.R., Mosley, A.N., Jun, S.J., Montanaro, F., Steffen, L.S., Zhou, Y., Nigro, V., Zon, L.I., Kunkel, L.M., 2005. Delta-sarcoglycan is required for early zebrafish muscle organization. Exp. Cell Res. 304, 105–115.

Guyon, J.R., Steffen, L.S., Howell, M.H., Pusack, T.J., Lawrence, C., Kunkel, L.M., 2007. Modeling human muscle disease in zebrafish. Biochim. Biophys. Acta 1772, 205–215.

Hartwig, J.H., Stossel, T.P., 1975. Isolation and properties of actin, myosin, and a new actinbinding protein in rabbit alveolar macrophages. J. Biol. Chem. 250, 5696–5705.

Hayashi, Y.K., Chou, F.L., Engvall, E., Ogawa, M., Matsuda, C., Hirabayashi, S., Yokochi, K., Ziober, B.L., Kramer, R.H., Kaufman, S.J., Ozawa, E., Goto, Y., Nonaka, I., Tsukahara, T., Wang, J.Z., Hoffman, E.P., Arahata, K., 1998. Mutations in the integrin alpha7 gene cause congenital myopathy. Nat. Genet. 19, 94–97.

Herman, I.M., 1993. Actin isoforms. Curr. Opin. Cell Biol. 5, 48–55.

Hoffman, E.P., Brown Jr., R.H., Kunkel, L.M., 1987. Dystrophin: the protein product of the Duchenne muscular dystrophy locus. Cell 51, 919–928.

Hyodo-Taguchi, Y., 1980. Establishment of inbred strains of the teleost, *Oryzias latipes*. Zool. Mag. 89, 283–301.

Inohaya, K., Yasumasu, S., Ishimaru, M., Ohyama, A., Iuchi, I., Yamagami, K., 1995. Temporal and spatial patterns of gene expression for the hatching enzyme in the teleost embryo, *Oryzias latipes*. Dev. Biol. 171, 374–385.

Inohaya, K., Yasumasu, S., Yasumasu, I., Iuchi, I., Yamagami, K., 1999. Analysis of the origin and development of hatching gland cells by transplantation of the embryonic shield in the fish, *Oryzias latipes*. Dev. Growth Differ. 41, 557–566.

Irwin, W.A., Bergamin, N., Sabatelli, P., Reggiani, C., Megighian, A., Merlini, L., Braghetta, P., Columbaro, M., Volpin, D., Bressan, G.M., Bernardi, P., Bonaldo, P., 2003.

Mitochondrial dysfunction and apoptosis in myopathic mice with collagen VI deficiency. Nat. Genet. 35, 367–371.
Ishikawa, Y., 1996. A recessive lethal mutation, tb, that bends the midbrain region of the neural tube in the early embryo of the medaka. Neurosci. Res. 24, 313–317.
Ishikawa, Y., 2000. Medakafish as a model system for vertebrate developmental genetics. Bioessays 22, 487–495.
Ishikawa, Y., Hyodo-Taguchi, Y., Aoki, K., Yasuda, T., Matsumoto, A., Sasanuma, M., 1999. Induction of mutations by ENU in the medaka germline. Fish Biol. J. Medaka 10, 27–29.
Iwamatsu, T., 2004. Stages of normal development in the medaka *Oryzias latipes*. Mech. Dev. 121, 605–618.
Kainulainen, T., Pender, A., D'Addario, M., Feng, Y., Lekic, P., McCulloch, C.A., 2002. Cell death and mechanoprotection by filamin A in connective tissues after challenge by applied tensile forces. J. Biol. Chem. 277, 21998–22009.
Kimura, T., Jindo, T., Narita, T., Naruse, K., Kobayashi, D., Shin, I.T., Kitagawa, T., Sakaguchi, T., Mitani, H., Shima, A., Kohara, Y., Takeda, H., 2004. Large-scale isolation of ESTs from medaka embryos and its application to medaka developmental genetics. Mech. Dev. 121, 915–932.
Kley, R.A., Hellenbroich, Y., van der Ven, P.F., Furst, D.O., Huebner, A., Bruchertseifer, V., Peters, S.A., Heyer, C.M., Kirschner, J., Schroder, R., Fischer, D., Muller, K., Tolksdorf, K., Eger, K., Germing, A., Brodherr, T., Reum, C., Walter, M.C., Lochmuller, H., Ketelsen, U.P., Vorgerd, M., 2007. Clinical and morphological phenotype of the filamin myopathy: a study of 31 German patients. Brain 130, 3250–3264.
Krakow, D., Robertson, S.P., King, L.M., Morgan, T., Sebald, E.T., Bertolotto, C., Wachsmann-Hogiu, S., Acuna, D., Shapiro, S.S., Takafuta, T., Aftimos, S., Kim, C.A., Firth, H., Steiner, C.E., Cormier-Daire, V., Superti-Furga, A., Bonafe, L., Graham Jr., J.M., Grix, A., Bacino, C.A., Allanson, J., Bialer, M.G., Lachman, R.S., Rimoin, D.L., Cohn, D.H., 2004. Mutations in the gene encoding filamin B disrupt vertebral segmentation, joint formation and skeletogenesis. Nat. Genet. 36, 405–410.
Lim, L.E., Duclos, F., Broux, O., Bourg, N., Sunada, Y., Allamand, V., Meyer, J., Richard, I., Moomaw, C., Slaughter, C., Tomé, F.M., Fardeau, M., Jackson, C.E., Beckmann, J.S., Campbell, K.P., 1995. Beta-sarcoglycan: characterization and role in limb-girdle muscular dystrophy linked to 4q12. Nat. Genet. 11, 257–265.
Linnemann, A., van der Ven, P.F., Vakeel, P., Albinus, B., Simonis, D., Bendas, G., Schenk, J.A., Micheel, B., Kley, R.A., Furst, D.O., 2010. The sarcomeric Z-disc component myopodin is a multiadapter protein that interacts with filamin and alpha-actinin. Eur. J. Cell Biol. 89, 681–692.
Loo, D.T., Kanner, S.B., Aruffo, A., 1998. Filamin binds to the cytoplasmic domain of the beta1-integrin. Identification of amino acids responsible for this interaction. J. Biol. Chem. 273, 23304–23312.
Lowe, T., Kley, R.A., van der Ven, P.F., Himmel, M., Huebner, A., Vorgerd, M., Furst, D.O., 2007. The pathomechanism of filaminopathy: altered biochemical properties explain the cellular phenotype of a protein aggregation myopathy. Hum. Mol. Genet. 16, 1351–1358.
Luan, X., Hong, D., Zhang, W., Wang, Z., Yuan, Y., 2010. A novel heterozygous deletion–insertion mutation (2695–2712 del/GTTTGT ins) in exon 18 of the filamin C gene causes filaminopathy in a large Chinese family. Neuromuscul. Disord. 20, 390–396.
Mayer, U., 2003. Integrins: redundant or important players in skeletal muscle? J. Biol. Chem. 278, 14587–14590.
Mayer, U., Saher, G., Fassler, R., Bornemann, A., Echtermeyer, F., von der Mark, H., Miosge, N., Poschl, E., von der Mark, K., 1997. Absence of integrin alpha 7 causes a novel form of muscular dystrophy. Nat. Genet. 17, 318–323.
Miosge, N., Klenczar, C., Herken, R., Willem, M., Mayer, U., 1999. Organization of the myotendinous junction is dependent on the presence of alpha7beta1 integrin. Lab. Invest. 79, 1591–1599.
Mizuno, Y., Noguchi, S., Yamamoto, H., Yoshida, M., Suzuki, A., Hagiwara, Y., Hayashi, Y.K., Arahata, K., Nonaka, I., Hirai, S., Ozawa, E., 1994. Selective defect of sarcoglycan complex in severe childhood autosomal recessive muscular dystrophy muscle. Biochem. Biophys. Res. Commun. 203, 979–983.
Nakata, T., Nishina, Y., Yorifuji, H., 2001. Cytoplasmic gamma actin as a Z-disc protein. Biochem. Biophys. Res. Commun. 286, 156–163.
Naruse, K., Fukamachi, S., Mitani, H., Kondo, M., Matsuoka, T., Kondo, S., Hanamura, N., Morita, Y., Hasegawa, K., Nishigaki, R., Shimada, A., Wada, H., Kusakabe, T., Suzuki, N., Kinoshita, M., Kanamori, A., Terado, T., Kimura, H., Nonaka, M., Shima, A., 2000. A detailed linkage map of medaka, *Oryzias latipes*: comparative genomics and genome evolution. Genetics 154, 1773–1784.
Nigro, V., de Sa Moreira, E., Piluso, G., Vainzof, M., Belsito, A., Politano, L., Puca, A.A., Passos-Bueno, M.R., Zatz, M., 1996. Autosomal recessive limb-girdle muscular dystrophy, LGMD2F, is caused by a mutation in the delta-sarcoglycan gene. Nat. Genet. 14, 195–198.
Noguchi, S., McNally, E.M., Ben Othmane, K., Hagiwara, Y., Mizuno, Y., Yoshida, M., Yamamoto, H., Bonnemann, C.G., Gussoni, E., Denton, P.H., Kyriakides, T., Middleton, L., Hentati, F., Ben Hamida, M., Nonaka, I., Vance, J.M., Kunkel, L.M., Ozawa, E., 1995. Mutations in the dystrophin-associated protein gamma-sarcoglycan in chromosome 13 muscular dystrophy. Science 270, 819–822.
Ohashi, K., Oshima, K., Tachikawa, M., Morikawa, N., Hashimoto, Y., Ito, M., Mori, H., Kuribayashi, T., Terasaki, A.G., 2005. Chicken gizzard filamin, retina filamin and cgABP260 are respectively, smooth muscle-, non-muscle- and pan-muscle-type isoforms: distribution and localization in muscles. Cell Motil. Cytoskeleton 61, 214–225.
Postel, R., Vakeel, P., Topczewski, J., Knoll, R., Bakkers, J., 2008. Zebrafish integrin-linked kinase is required in skeletal muscles for strengthening the integrin-ECM adhesion complex. Dev. Biol. 318, 92–101.
Roberds, S.L., Leturcq, F., Allamand, V., Piccolo, F., Jeanpierre, M., Anderson, R.D., Lim, L.E., Lee, J.C., Tomé, F.M., Romero, N.B., Fardeau, M., Beckmann, J.S., Kaplan, J.C., Campbell, K.P., 1994. Missense mutations in the adhalin gene linked to autosomal recessive muscular dystrophy. Cell 78, 625–633.
Robertson, S.P., Twigg, S.R., Sutherland-Smith, A.J., Biancalana, V., Gorlin, R.J., Horn, D., Kenwrick, S.J., Kim, C.A., Morava, E., Newbury-Ecob, R., Orstavik, K.H., Quarrell, O.W., Schwartz, C.E., Shears, D.J., Suri, M., Kendrick-Jones, J., Wilkie, A.O., 2003. Localized mutations in the gene encoding the cytoskeletal protein filamin A cause diverse malformations in humans. Nat. Genet. 33, 487–491.
Rybakova, I.N., Patel, J.R., Ervasti, J.M., 2000. The dystrophin complex forms a mechanically strong link between the sarcolemma and costameric actin. J. Cell Biol. 150, 1209–1214.
Samitt, C.E., Bonilla, E., 1990. Immunocytochemical study of dystrophin at the myotendinous junction. Muscle Nerve 13, 493–500.
Sehnert, A.J., Huq, A., Weinstein, B.M., Walker, C., Fishman, M., Stainier, D.Y., 2002. Cardiac troponin T is essential in sarcomere assembly and cardiac contractility. Nat. Genet. 31, 106–110.
Selcen, D., 2008. Myofibrillar myopathies. Curr. Opin. Neurol. 21, 585–589.
Selcen, D., Ohno, K., Engel, A.G., 2004. Myofibrillar myopathy: clinical, morphological and genetic studies in 63 patients. Brain 127, 439–451.
Shatunov, A., Olive, M., Odgerel, Z., Stadelmann-Nessler, C., Irlbacher, K., van Landeghem, F., Bayarsaikhan, M., Lee, H.S., Goudeau, B., Chinnery, P.F., Straub, V., Hilton-Jones, D., Damian, M.S., Kaminska, A., Vicart, P., Bushby, K., Dalakas, M.C., Sambuughin, N., Ferrer, I., Goebel, H.H., Goldfarb, L.G., 2009. In-frame deletion in the seventh immunoglobulin-like repeat of filamin C in a family with myofibrillar myopathy. Eur. J. Hum. Genet. 17, 656–663.
Shifrin, Y., Arora, P.D., Ohta, Y., Calderwood, D.A., McCulloch, C.A., 2009. The role of FilGAP–filamin A interactions in mechanoprotection. Mol. Biol. Cell 20, 1269–1279.
Shimizu, T., Matsumura, K., Sunada, Y., Mannen, T., 1989. Dense immunostainings on both neuromuscular and myotendon junction with an anti-dystrophin monoclonal antibody. Biomed. Res. 10, 405–409.
Steffen, L.S., Guyon, J.R., Vogel, E.D., Beltre, R., Pusack, T.J., Zhou, Y., Zon, L.I., Kunkel, L.M., 2007. Zebrafish orthologs of human muscular dystrophy genes. BMC Genomics 8, 79.
Stossel, T.P., Condeelis, J., Cooley, L., Hartwig, J.H., Noegel, A., Schleicher, M., Shapiro, S.S., 2001. Filamins as integrators of cell mechanics and signalling. Nat. Rev. Mol. Cell Biol. 2, 138–145.
Stossel, T.P., Hartwig, J.H., 1975. Interactions between actin, myosin, and an actin-binding protein from rabbit alveolar macrophages. Alveolar macrophage myosin Mg^{2+}-adenosine triphosphatase requires a cofactor for activation by actin. J. Biol. Chem. 250, 5706–5712.
Summers, A.P., Koob, T.J., 2002. The evolution of tendon – morphology and material properties. Comp. Biochem. Physiol. A Mol. Integr. Physiol. 133, 1159–1170.
Telfer, W.R., Busta, A.S., Bonnemann, C.G., Feldman, E.L., Dowling, J.J., 2010. Zebrafish models of collagen VI-related myopathies. Hum. Mol. Genet. 19, 2433–2444.
Thompson, T.G., Chan, Y.M., Hack, A.A., Brosius, M., Rajala, M., Lidov, H.G., McNally, E.M., Watkins, S., Kunkel, L.M., 2000. Filamin 2 (FLN2): a muscle-specific sarcoglycan interacting protein. J. Cell Biol. 148, 115–126.
van der Flier, A., Gaspar, A.C., Thorsteinsdottir, S., Baudoin, C., Groeneveld, E., Mummery, C.L., Sonnenberg, A., 1997. Spatial and temporal expression of the beta1D integrin during mouse development. Dev. Dyn. 210, 472–486.
van der Ven, P.F., Obermann, W.M., Lemke, B., Gautel, M., Weber, K., Furst, D.O., 2000a. Characterization of muscle filamin isoforms suggests a possible role of gamma-filamin/ABP-L in sarcomeric Z-disc formation. Cell Motil. Cytoskeleton 45, 149–162.
van der Ven, P.F., Wiesner, S., Salmikangas, P., Auerbach, D., Himmel, M., Kempa, S., Hayess, K., Pacholsky, D., Taivainen, A., Schroder, R., Carpen, O., Furst, D.O., 2000b. Indications for a novel muscular dystrophy pathway. gamma-filamin, the muscle-specific filamin isoform, interacts with myotilin. J. Cell Biol. 151, 235–248.
Vorgerd, M., van der Ven, P.F., Bruchertseifer, V., Lowe, T., Kley, R.A., Schroder, R., Lochmuller, H., Himmel, M., Koehler, K., Furst, D.O., Huebner, A., 2005. A mutation in the dimerization domain of filamin c causes a novel type of autosomal dominant myofibrillar myopathy. Am. J. Hum. Genet. 77, 297–304.
Wada, H., Shimada, A., Fukamachi, S., Naruse, K., Shima, A., 1998. Sex-linked inheritance of the lf locus in the medaka fish (*Oryzias latipes*). Zoolog. Sci. 15, 123–126.
Watkins, S.C., Hoffman, E.P., Slayter, H.S., Kunkel, L.M., 1988. Immunoelectron microscopic localization of dystrophin in myofibres. Nature 333, 863–866.
Wittbrodt, J., Shima, A., Schartl, M., 2002. Medaka—a model organism from the far East. Nat. Rev. Genet. 3, 53–64.
Xu, X., Meiler, S.E., Zhong, T.P., Mohideen, M., Crossley, D.A., Burggren, W.W., Fishman, M.C., 2002. Cardiomyopathy in zebrafish due to mutation in an alternatively spliced exon of titin. Nat. Genet. 30, 205–209.
Yoshida, M., Hama, H., Ishikawa-Sakurai, M., Imamura, M., Mizuno, Y., Araishi, K., Wakabayashi-Takai, E., Noguchi, S., Sasaoka, T., Ozawa, E., 2000. Biochemical evidence for association of dystrobrevin with the sarcoglycan–sarcospan complex as a basis for understanding sarcoglycanopathy. Hum. Mol. Genet. 9, 1033–1040.

サルコメア配列異常を主病変とする筋ジストロフィーの

病因・病態の解明と治療法の開発

Available online at www.sciencedirect.com

SciVerse ScienceDirect

Neuromuscular Disorders 22 (2012) 162–165

www.elsevier.com/locate/nmd

Case report

Muscle glycogen storage disease 0 presenting recurrent syncope with weakness and myalgia

Sayuri Sukigara [a], Wen-Chen Liang [b,c], Hirofumi Komaki [a], Tokiko Fukuda [d], Takeshi Miyamoto [e], Takashi Saito [a], Yoshiaki Saito [a], Eiji Nakagawa [a], Kenji Sugai [a], Yukiko K. Hayashi [b], Hideo Sugie [d], Masayuki Sasaki [a], Ichizo Nishino [b,*]

[a] *Department of Child Neurology, National Center Hospital, National Center of Neurology and Psychiatry (NCNP), Kodaira, Tokyo, Japan*
[b] *Department of Neuromuscular Research, National Institute of Neuroscience, NCNP, Kodaira, Tokyo, Japan*
[c] *Department of Pediatrics, Kaohsiung Medical Univeristy Hospital, Kaohsiung Medical University, Kaohsiung, Taiwan*
[d] *Department of Pediatrics, Jichi Medical University and Jichi Chidren's Medical Center, Shimotsuke, Tochigi, Japan*
[e] *Department of Pediatrics, Kosai Municipal Hospital, Kosai, Shizuoka, Japan*

Received 22 March 2011; received in revised form 17 June 2011; accepted 22 August 2011

Abstract

Muscle glycogen storage disease 0 (GSD0) is caused by glycogen depletion in skeletal and cardiac muscles due to deficiency of glycogen synthase 1 (GYS1), which is encoded by the *GYS1* gene. Only two families with this disease have been identified. We report a new muscle GSD0 patient, a Japanese girl, who had been suffering from recurrent attacks of exertional syncope accompanied by muscle weakness and pain since age 5 years until she died of cardiac arrest at age 12. Muscle biopsy at age 11 years showed glycogen depletion in all muscle fibers. Her loss of consciousness was gradual and lasted for hours, suggesting that the syncope may not be simply caused by cardiac event but probably also contributed by metabolic distress.

Keywords: Glycogen storage disease; Glycogen synthase; Glycogen; Syncope; Sudden death

1. Introduction

Glycogen is a high molecular mass polysaccharide that serves as a repository of glucose for use in times of metabolic need. It is stored in liver, cardiac and skeletal muscles, and broken down to glucose to produce ATP as energy as needed. For the synthesis of glycogen, at least two proteins, glycogenin (GYG) and glycogen synthase (GYS), are known to be essential. GYG is involved in the initiation reactions of glycogen synthesis: the covalent attachment of a glucose residue to GYG is followed by elongation to form an oligosaccharide chain [1]. GYS catalyzes the addition of glucose monomers to the growing glycogen molecule through the formation of alpha-1,4-glycoside linkages [2].

Defect in either GYG or GYS can cause glycogen depletion. Recently, muscle glycogen deficiency due to a mutation in a gene encoding muscle GYG, *GYG1*, was reported [3] and named as glycogen storage disease type XV. In contrast, glycogen depletion caused by the *GYS* gene mutation is called glycogen storage disease type 0 (GSD0). GSD0 was first reported in 1990 in patients with type 2 diabetes who had a defect in glycogen synthesis in liver, which was caused by a defect in liver GYS, GYS2, and the disease was named as liver GSD0 (or also called GSD0a) [4,5].

The disease of muscle GYS, GYS1, was first described in 2007 in three siblings and named muscle GSD0, which is

* Corresponding author. Address: Department of Neuromuscular Research, National Institute of Neuroscience, NCNP, 4-1-1, Ogawahigashi-cho, Kodaira, Tokyo 187 8551, Japan. Tel.: +81 42 3412711; fax: +81 42 3427521.
E-mail address: nishino@ncnp.go.jp (I. Nishino).

0960-8966/$ - see front matter © 2011 Elsevier B.V. All rights reserved.
doi:10.1016/j.nmd.2011.08.008

also called GSD0b [6]. One of the patients initially manifested exercise intolerance, epilepsy and long QT syndrome since the age of 4 years, then died of sudden cardiac arrest after exertion when he was 10.5-year-old. The other two siblings were then genetically confirmed as muscle GSD0 with mutations in *GYS1* and cardiac involvement was also found in both. The second muscle GSD0 family was reported in 2009 [7]. The 8-year-old boy had been healthy before collapsing during a bout of exercise, resulting in death. Post-mortem examinations and studies verified the diagnosis of muscle GSD0. He had a female sibling who died at 6 days of age of undetermined cause. Here we report the first muscle GSD0 patient in Asia with some distinct clinical manifestations from other reported cases.

2. Case report

An 11-year-old Japanese girl with repeated episodes of post-exercise loss of consciousness, weakness, and myalgia since age 5 years, was admitted to the hospital. She was the first child of unrelated healthy parents. She was born uneventfully and was normal in psychomotor development. At age 2 years, she developed the first episode of generalized tonic-clonic seizure while she was sleeping. At age 4 years, she had the second episode of generalized tonic-clonic seizure when she was under general anesthesia for tonsillectomy, whose cause was thought to be hypoglycemia due to prolonged fasting. In both episodes, seizure was followed by strong limb pain. At age 5 years, she suffered from the first episode of syncope while climbing up stairs. She recovered after a few hours. One year later, she had the second syncopal attack after running 50 m, which was accompanied by subsequent limb muscle weakness and myalgia. Since then, similar episodes were repeated several times a year. For each bout, she first developed leg muscle weakness immediately after exercise, making her squat down, and gradually lost the consciousness. She recovered her consciousness after a few hours but always experienced strong myalgia in legs which lasted for several hours. Blood glucose level was not decreased during these attacks.

On admission, general physical examination revealed no abnormal finding. On neurological examination, she had mild proximal dominant muscle weakness and mildly limited dorsiflexion of both ankle joints. T1-weighted images of skeletal muscle MRI showed high signal intensities in gluteal and flexor muscles of the thigh, which were assessed to be fatty degeneration (Fig. 1). Systemic investigations including electrocardiography, echocardiography, stress cardiac catheterization, stress myocardial scintigraphy, brain imaging, electroencephalography, and screening tests for metabolic diseases revealed no abnormality except for a mild ischemic finding on exercise electrocardiography. Ischemic and non-ischemic forearm exercise tests [8] showed the lack of lactate elevation, raising a possibility of glycogen storage disease. A few months later, resting electrocardiography, 24-h holter monitoring and resting echocardiography were re-evaluated and again revealed normal findings.

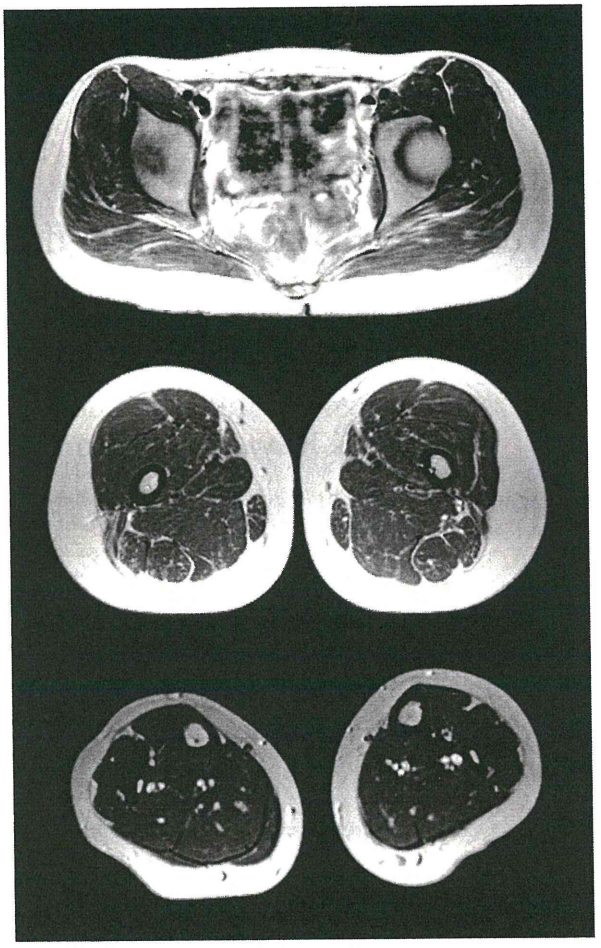

Fig. 1. Muscle MRI, T2WI, axial. It shows high intensity in gluteus maximus and biceps femoris muscles.

3. Histological analysis of skeletal muscle

Muscle biopsy was performed from biceps brachii. Serial frozen sections were stained with hematoxylin and eosin, modified Gomori trichrome, and a battery of histochemical methods. The most striking finding was depletion of glycogen in all muscle fibers but not in the interstitium on periodic acid-schiff (PAS) staining (Fig. 2A). Phosphorylase activity was also deficient in all fibers (Fig. 2B). Mitochondria especially at the periphery of muscle fibers were prominent on modified Gomori trichrome (Fig. 2D). ATPase staining revealed type 2 fiber atrophy. Electron microscopic analysis showed mitochondrial proliferation at the periphery of muscle fibers with no notable intramitochondrial inclusions (Fig. 2E).

4. Biochemical and molecular analysis

Both the activity of GYS1 and the amount of glycogen in the skeletal muscle were markedly reduced (Table 1). On western blotting, GYS1 in the patient's skeletal muscle was undetectable (Fig. 2F). The *GYS1* gene sequence analysis revealed compound heterozygous mutation of

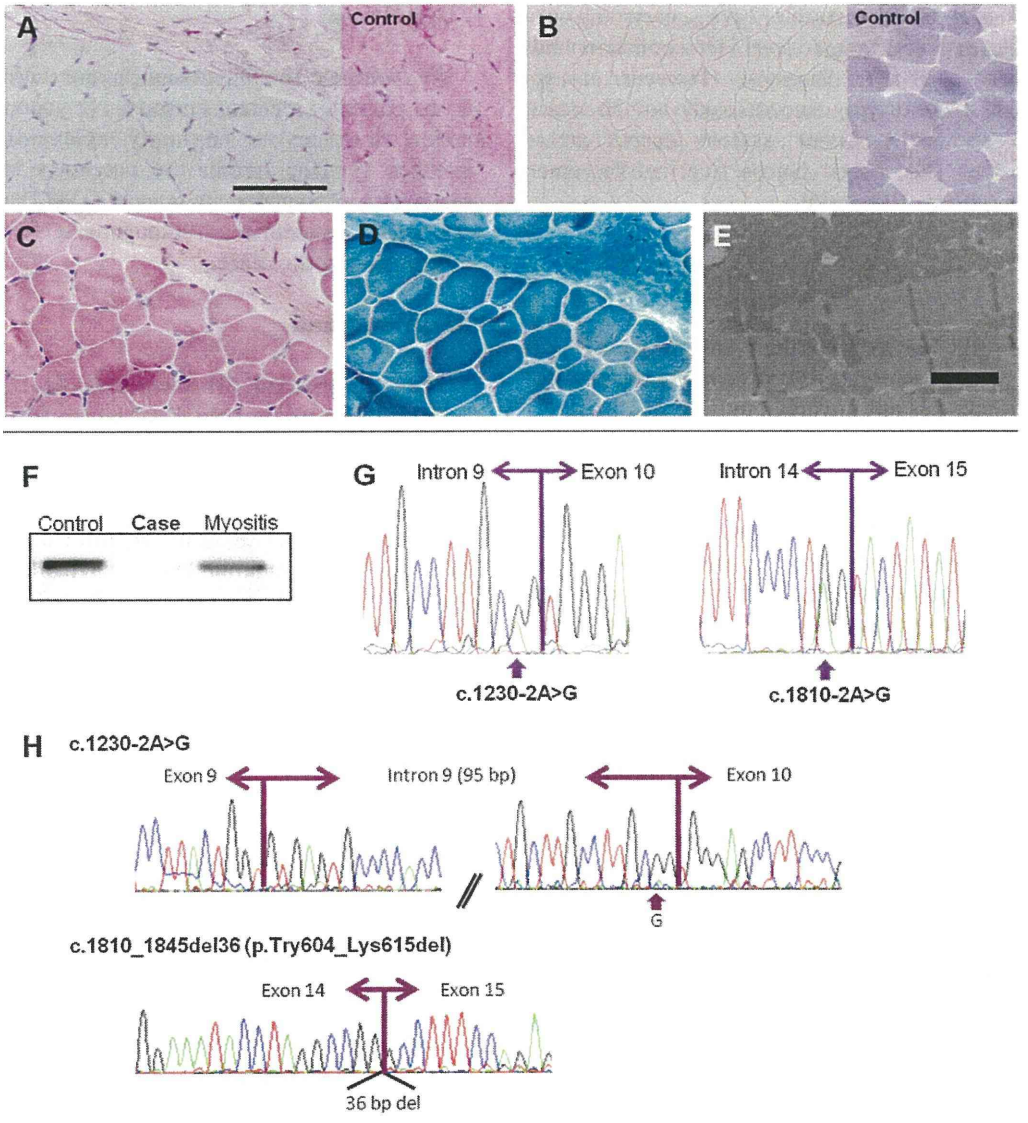

Fig. 2. Histological, genetic and protein analyses. Periodic acid-schiff (PAS) staining shows marked depletion of glycogen in muscle fibers but not in the interstitium (A). Phosphorylase activity is also deficient in all fibers (B). Hematoxylin and eosin staining shows mild fiber size variation (C). On modified Gomori trichrome, mitochondria are prominent especially at the margin of each muscle fiber (D). On electron microscopy (EM), mitochondria are increased in number at the periphery of muscle fibers (E). Bars represent 100 μm for histochemistry and 7 μm for EM. On western blotting using anti-GYS1 antibody (Abcam), GYS1 protein is absent in skeletal muscle from the patient (F). Sequence analysis for the *GYS1* gene reveals a compound heterozygous mutation of c.1230-2A > G and c.1810-2A > G (G). cDNA analysis showed insertion of intron 9 between exon 9 and 10 and 36-bp deletion from the beginning of exon 15 (H).

Table 1
Analyses of enzymatic activity and glycogen content. The activity of GYS and glycogen content in skeletal muscle were markedly reduced.

	Glycogen synthase (mol/min/mg)	UDPG-pyrophosphorylase (nmol/min/mg)	Glycogen contents (% of wet weight)
Patient	*0.9*	30.5	*0.03*
Control	42.0 ± 11.2	31.2 ± 3.5	0.94 ± 0.55

Italicized values: lower than control range.

c.1230-2A > G in intron 9 and c.1810-2A > G in intron 14 (Fig. 2G). cDNA analysis confirmed the insertion of the full-length intron 9 between exons 9 and 10 and a 36-bp deletion in the beginning of exon 15 (Fig. 2H).

5. Clinical course after diagnosis

Upon the diagnosis of GSD0, exercise was strictly limited to avoid syncope resulted from glucose depletion. In

addition, oral intake of cornstarch (2 g/kg, every 6 h) was started to maintain blood sugar level. Her condition had been stable for 1 year after diagnosis. However, at age 12 years, she was found lying unconsciously on the stairs at her school. She had persistent asystole despite ambulance resuscitation. The blood glucose level in the emergency room was above 100 mg/dl.

6. Discussion

We identified the first Asian patient with muscle GSD0, who manifested recurrent episodes of syncope with subsequent muscle weakness and myalgia, and eventually developed cardiac arrest.

Findings in our patient seem to be similar to previous reports, but some differences indicated the possibility of another pathogenesis of the disease. Our patient repeatedly suffered from episodes of syncope. In contrast to two earlier reports, those patients never had syncope, although the last attack led to sudden death [6,7]. In support of this notion, most muscle glycogen synthase knock-out mice died soon after birth due to impaired cardiac function [8]. However, the pattern of loss of consciousness in our patient cannot be explained by simple cardiac dysfunction, as she lost her consciousness gradually after exercise and took hours to regain, which is different from typical cardiac syncope, usually showing sudden loss of consciousness and rapid recovery. Alternatively, defective glycogen synthesis in brain may be related to syncope, as GYS1 is also expressed in brain, albeit not so much as in cardiac and skeletal muscles. Another possibility may be intermittent arrhythmia. However, electrocardiogram during the episode was never obtained. Further studies are necessary to answer this question.

On muscle pathology and electron microscopy, we found profound deficiency of glycogen in all muscle fibers accompanied by mitochondrial proliferation, which is similar to previous reports. The mitochondrial proliferation may reflect a compensatory mechanism for supplying ATP to glycogen-depleted muscles. Interestingly, phosphorylase activity on histochemistry seemed deficient. This is consistent with the fact that endogenous glycogen is used as a substrate of phosphorylase on histochemistry. Previous reports described the reduced number of type 2 fibers. In our patient, type 2 fiber atrophy, but not type 2 fiber deficiency, was seen. Although type 2 fiber atrophy is a nonspecific finding, this picture might also reflect the dysfunction of glycogen-dependent muscle fibers.

7. Conclusion

We identified the first Asian patient with muscle GSD0. In our patient, recurrent episodes of syncope and eventual sudden death may not be simply explained by cardiac dysfunction. Further studies are necessary to elucidate the mechanism of syncope in muscle GSD0 and to establish appropriate guideline of management for these patients to prevent sudden death.

Acknowledgments

The authors thank Ms. Goto and Ms. Ogawa (National Center of Neurology and Psychiatry) for technical assistance in mutation analysis. This work is supported by: a Grant-in-Aid for Scientific Research from Japan Society for the Promotion of Science; Research on Psychiatric and Neurological Diseases and Mental Health, Research on Measures for Intractable Diseases, Health Labour Sciences Research Grant for Nervous and Mental Disorders (20B-12, 20B-13) from the Ministry of Health, Labor, and Welfare, and Intramural Research Grant (23-4, 23-5, 23-6) for Neurological and Psychiatric Disorders of NCNP.

References

[1] Viskupic E, Cao Y, Zhang W, Cheng C, DePaoli-Roach AA. Roach PJ. J Biol Chem 1992;267:25759–63.
[2] Pederson BA et al. Abnormal cardiac development in the absence of heart glycogen. Mol Cell Biol 2004;24:7179–87.
[3] Moslemi AR, Lindberg C, Nilsson J, Tajsharghi H, Andersson B, Oldfors A. Glycogenin-1 deficiency and inactivated priming of glycogen synthesis. N Eng J Med 2010;362:1203–10.
[4] Shulman GI, Rothman DI, Jue T, Stein P, DeFronzo PA, Shulman RG. Quantitation of muscle glycogen synthesis in normal subjects and subjects with non-insulin-dependent diabetes by 13C nuclear magnetic resonance spectroscopy. N Eng J Med 1990;322:223–8.
[5] Orho M, Bosshard NU, Buist NR, Gitzelmann R, Aynsley-Green A, Blümel P, et al. Mutations in the liver glycogen synthase gene in children with hypoglycemia due to glycogen storage disease type 0. J Clin Invest 1998;102:507–15.
[6] Kollberg G, Tulinius M, Gilljam T, Ostman-Smith I, Forsander G, Jotorp P, et al. Cardiomyopathy and exercise intolerance in muscle glycogen storage disease 0. N Engl J Med 2007;357:1507–14.
[7] Cameron JM, Levandovskiy V, MacKay N, Utgiker R, Ackerley C, Chiasson D, et al. Identification of a novel mutation in *GYS1* (muscle-specific glycogen synthase) resulting in sudden cardiac death, that is diagnosable from skin fibroblasts. Mol Genet Metab 2009;98:378–82.
[8] Pederson BA, Cope CR, Schroeder JM, Smith NW, Irimia JM, Thurberg BL, et al. Exercise capacity of mice genetically lacking muscle glycogen synthase: in mice, muscle glycogen is not essential for exercise. J Biol Chem 2005;280:17260–5.

European Journal of Neurology 2012, 19: 501–509 doi:10.1111/j.1468-1331.2011.03575.x

EUROPEAN JOURNAL OF NEUROLOGY
THE OFFICIAL JOURNAL OF THE EUROPEAN FEDERATION OF NEUROLOGICAL SOCIETIES

Characterization of the Asian myopathy patients with *VCP* mutations

Z. Shi[a], Y. K. Hayashi[a], S. Mitsuhashi[a], K. Goto[a], D. Kaneda[b], Y.-C. Choi[c], C. Toyoda[d], S. Hieda[e], T. Kamiyama[f], H. Sato[g], M.Wada[g], S. Noguchi[a], I. Nonaka[a] and I. Nishino[a]

[a]*Department of Neuromuscular Research, National Institute of Neuroscience, National Center of Neurology and Psychiatry (NCNP), Kodaira, Tokyo;* [b]*Department of Neurology, Osaka Red Cross Hospital, Osaka, Japan;* [c]*Department of Neurology, Gangnam Severance Hospital, Yonsei University College of Medicine, Seoul, Korea;* [d]*Department of Neurology, Daisan Hospital, Jikei Medical University, Tokyo;* [e]*Department of Neurology, Showa Medical University, Tokyo;* [f]*Department of Neurology, Jikei Medical University, Tokyo; and* [g]*Department of Neurology, Hematology, Metabolism, Endocrinology and Diabetology, Faculty of Medicine, Yamagata University, Yamagata, Japan*

Keywords:
amyotrophic lateral sclerosis, cytoplasmic inclusion, inclusion body myopathy with Paget's disease of bone and frontotemporal dementia, rimmed vacuolar myopathy, nuclear inclusion, transactivation response DNA-binding protein 43, ubiquitin, valosin-containing protein

Received 8 August 2011
Accepted 15 September 2011

Background and purpose: Mutations in the valosin-containing protein (*VCP*) gene are known to cause inclusion body myopathy with Paget's disease of bone and frontotemporal dementia (IBMPFD) and familial amyotrophic lateral sclerosis (ALS). Despite an increasing number of clinical reports, only one Asian family with IBMPFD has been described.

Methods: To characterize patients with *VCP* mutations, we screened a total of 152 unrelated Asian families who were suspected to have rimmed vacuolar myopathy.

Results: We identified *VCP* mutations in seven patients from six unrelated Asian families. Five different missense mutations were found, including a novel p.Ala439Pro substitution. All patients had adult-onset progressive muscle wasting with variable involvement of axial, proximal, and distal muscles. Two of seven patients were suggested to have mild brain involvement including cerebellar ataxia, and only one showed radiological findings indicating a change in bone. Findings from skeletal muscle indicated mixed neurogenic and myogenic changes, fibers with rimmed vacuoles, and the presence of cytoplasmic and nuclear inclusions. These inclusions were immunopositive for VCP, ubiquitin, transactivation response DNA-binding protein 43, and also histone deacetylase 6 (HDAC6), of which function is regulated by VCP. Evidence of early nuclear and mitochondrial damage was also characteristic.

Conclusions: Valosin-containing protein mutations are not rare in Asian patients, and gene analysis should be considered for patients with adult-onset rimmed vacuolar myopathy with neurogenic changes. A wide variety of central and peripheral nervous system symptoms coupled with rare bone abnormalities may complicate diagnosis.

Introduction

Mutations in the valosin-containing protein (*VCP*) gene on chromosome 9p13-p12 are known to cause an autosomal dominant multisystem disorder referred to as inclusion body myopathy with Paget's disease of bone (PDB) and frontotemporal dementia (IBMPFD) [1]. Myopathy is the most common clinical symptom observed in 90% of affected individuals, and this usually appears when patients are in their 40s. About 30% of IBMPFD patients show only muscle symptoms. Characteristic pathology findings include the presence of VCP- and ubiquitin-positive cytoplasmic and nuclear inclusions together with rimmed vacuoles in skeletal muscle. Accumulation of transactivation response DNA-binding protein 43 (TDP-43), a VCP-interacting protein, is also characteristic. PDB is observed in about a half of the IBMPFD patients at approximately the same age that the myopathy typically appears, whereas frontotemporal dementia (FTD) is seen in 32% with an age of onset that is nearly 10 years later than either the myopathy or PDB [2]. Nuclear VCP- and ubiquitin-positive inclusions are also seen in neurons [3]. Recently, *VCP* mutations were identified in five families

Correspondence: Y. K. Hayashi, Department of Neuromuscular Research, National Institute of Neuroscience, National Center of Neurology and Psychiatry (NCNP), 4-1-1, Ogawa-Higashi, Kodaira, Tokyo 187-8502, Japan (tel.: +81 42 341 2711 ext. 5113; fax: +81 42 346 1742; e-mail: hayasi_y@ncnp.go.jp).

with amyotrophic lateral sclerosis (ALS) [4]. Although nearly 50 families with *VCP* mutations have been reported worldwide, only one such family has been recently identified from an East Asian population [5]. Here, we identified seven Asian patients in six unrelated families with mutations in *VCP* and performed detailed clinical and pathological analyses.

Methods

All clinical materials used in this study were obtained for diagnostic purposes with written informed consent. All experiments performed in this study were approved by the Ethical Committee of the National Center of Neurology and Psychiatry.

Patients

The presence of rimmed vacuoles is a characteristic pathological finding for IBMPFD. We performed *VCP* mutation screening in a total of 152 unrelated Asian families who were suspected to have rimmed vacuolar myopathy. Eighty-seven patients had distal myopathy with rimmed vacuoles/hereditary inclusion body myopathy (DMRV/hIBM) with no glucosamine (UDP-*N*-acetyl)-2-epimerase/*N*-acetylmannosamine kinase (*GNE*) mutations. Twenty-five cases of limb-girdle muscular dystrophy (LGMD) of unknown cause and 40 other undiagnosed myopathy cases were also included in which patients' muscle contained rimmed vacuoles.

Mutation analysis

Genomic DNA was isolated from peripheral lymphocytes or muscle specimens by using standard techniques. All 17 exons and their flanking intronic regions of *VCP* were sequenced directly using an ABI PRISM 3130 automated sequencer (PE Applied Biosystems, CA, USA). Primer sequences are available on request. For the identification of novel nucleotide changes, 100 control chromosomes were screened.

Muscle pathology

Biopsied skeletal muscles were frozen with isopentane cooled in liquid nitrogen. Frozen serial sections of 10 μm thickness were stained using various conventional histochemical methods, including hematoxylin and eosin, modified Gomori trichrome, and cytochrome *c* oxidase (COX), which reflect a mitochondrial electron transport enzyme activity. To know the fiber type distribution and their composition, ATPase stains under different pH were performed.

Immunohistochemistry was performed using standard protocols. Antibodies using in this study were listed in Table S1. The sections were observed with epifluorescence using an Axiophoto2 microscope (Carl Zeiss, Oberkochen, Germany). To detect apoptotic nuclei, a fluorometric terminal dUTP nick-end labeling (TUNEL) detection kit (Takara Bio Int., Shiga, Japan) was used according to the manufacturer's instructions.

Electron microscopy

Biopsied specimens were fixed in 2.5% glutaraldehyde and post-fixed with 2% osmium tetroxide. Semithin sections stained with toluidine blue were examined by light microscopy. Ultrastructural analysis was carried out on ultrathin sections of muscles after staining with uranyl acetate and lead citrate, using a transmission electron microscope (JEM 1400; Jeol, Tokyo, Japan).

Results

Mutation analysis of *VCP*

We identified five different heterozygous missense mutations in seven patients, including c.277C > T (p.Arg93Cys) in Patient 1, c.463C > T (p.Arg155Cys) in Patients 2 and 3 (unrelated), c.464G > A (p.Arg155His) in Patient 4, c.572G > A (p.Arg191Gln) in Patient 5, and c.1315G > C (p.Ala439Pro) in Patients 6 and 7 (from the same family). The novel c.1315G > C mutation was not found in 100 Japanese control chromosomes, and p.Ala439 is conserved among species (Fig. 1).

Clinical findings

Clinical information of each patient is summarized in Table 1. All seven patients had adult-onset slowly progressive muscle weakness and atrophy with variable involvement of axial, proximal, and distal muscles. Two patients (Patients 5 and 6) showed asymmetrical involvement at the onset of the disease. Muscle pain, cramps, and fasciculations were often observed. Serum creatine kinase (CK) levels were normal to mildly elevated. Electromyography (EMG) showed mixed findings with neurogenic and myogenic changes, and nerve conduction velocity was decreased in two patients (Patients 3 and 4).

Only one patient (Patient 7) had an irregular sclerotic region in the 5th lumbar vertebral body with normal serum alkaline phosphatase level. Increased urine deoxypyridinoline level, a specific marker for bone resorption, was observed in Patient 2 with normal bone images. The other patients showed no signs suggesting bone involvement.

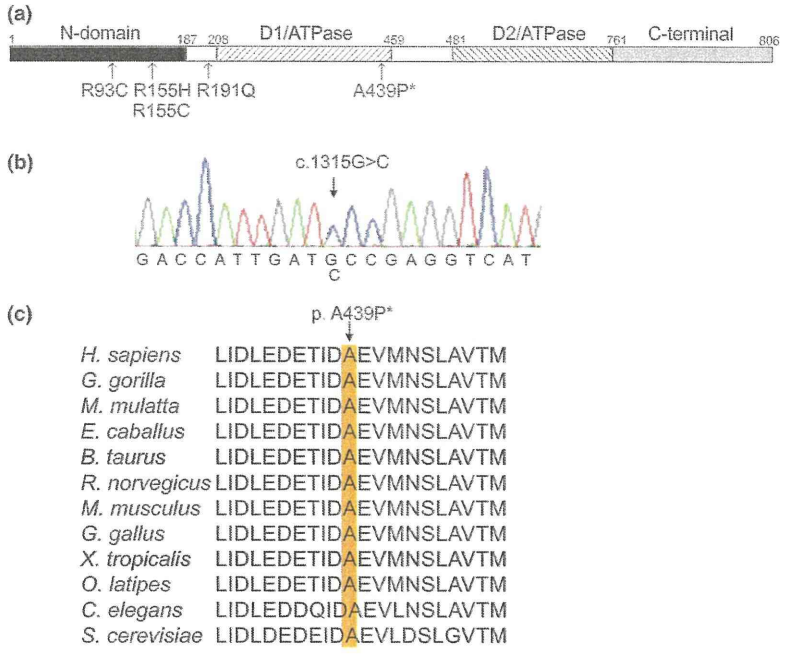

Figure 1 Result of valosin-containing protein (VCP) mutation screening. (a) The domain structure of human *VCP* (modified from Guinto *et al.* [28]) and position of the mutations identified in our series. (b) A novel heterozygous c.1315G > C substitution (p. Ala439Pro) is seen in Patients 6 and 7. (c) The alanine residue at position 439 (orange) is well preserved among the species including *Saccharomyces cerevisiae*.

Two of seven patients (Patients 2 and 7) showed mild cognitive impairment. Importantly, Patient 2, whose deceased brother had a diagnosis of spinocerebellar degeneration, showed signs of cerebellar involvement prior to impairment of frontal function, including dysarthria, symmetrical muscle hypotonia, and mild ataxia.

Muscle pathology

Skeletal muscle tissues from all seven patients with *VCP* mutations (Patients 2–7) showed mixed changes indicating myopathy and neuropathy. Scattered fibers with rimmed vacuoles were commonly seen (Fig. 2a and b). Cytoplasmic bodies were also seen in some fibers, with or without rimmed vacuoles (Fig. 2b). In addition, small angular fibers, groups of atrophic fibers, and fiber type grouping were seen. An increased number of type 2C fibers suggested presence of immature fibers or active fiber type conversion (Fig. 2a and c). Some fibers showed deficiency of COX stain, which reflect a mitochondrial electron transport enzyme activity (Fig. 2d). Succinate dehydrogenase (SDH) is a mitochondrial enzyme complex which demonstrates the relative proportions of mitochondria in muscle fibers. SDH staining of these COX-deficient fibers was variable from irregularly intense to negative (data not shown).

Immunohistochemical analysis was performed in muscle tissue from four patients with *VCP* mutations (Patients 2, 3, 4 and 6), together with samples from 10 DMRV, and eight sporadic inclusion body myositis (sIBM) patients. In normal skeletal muscle, TDP-43 is clearly detected in the nuclei (Fig. 3a). Nuclei in DMRV/hIBM and sIBM muscles were also strongly stained with TDP-43 (Figs 3c and d). In contrast, samples taken from patients with *VCP* mutations showed many nuclei with a deficiency of TDP-43 staining (Figs 3b, 4a and d). Besides, some TDP-43-positive nuclei were enlarged and costained with ubiquitin (Fig. 4a–d). These findings were commonly seen in all four patients with *VCP* mutations. Some ubiquitin- and TDP-43-positive myonuclei were also seen in DMRV/hIBM and sIBM muscles (data not shown).

The presence of nuclear inclusions stained with VCP is a characteristic finding of muscle from patients with *VCP* mutations. These VCP-positive nuclei were observed in all four patients with *VCP* mutations from 1.0 to 6.6% of myonuclei and costained with ubiquitin (Figs 3f and 4e–h). Some nuclei were also positive for histone deacetylase 6 (HDAC6) (Fig. 4j–k). The VCP-positive nuclei were not seen in muscle from patients with DMRV/hIBM or sIBM. Only a few nuclei were positive for TUNEL in all of the diseased muscle specimens examined (data not shown).

On the other hand, ubiquitin-positive cytoplasmic inclusions were observed in muscles from all patients with *VCP* mutations we examined varying from 6 to 25% of the muscle fibers (Fig. 4b). These cytoplasmic inclusions were often seen beside the nucleus and costained with TDP-43 (Fig. 4a–d), VCP (Fig. 4i), HDAC6 (Fig. 4j–l), p62, and SMI-31 (data not shown). In muscle tissue from patients with DMRV/hIBM or sIBM, scattered ubiquitin-positive, and a few

Table 1 Clinical summary of the patients

Pt No.	Sex/age (years)	Age at onset (years)	Clinical diagnosis	Affected relatives (diagnosis)	Initial symptom	Muscle weakness	CK (IU/L)	EMG	Muscle biopsy	*VCP* mutation	Bone Involve	Brain Involve
1	M/70	58	DMRV	Brother (DMRV)	Dragging gait	Four limbs (P > D, L = U), neck flexion	286	Myo/ Neuro	ND	R93C	No	No
2	F/57	47	DMRV/ IBMPFD	Brother (SCD)	Weakness of lower limbs	Paraspinal, four limbs (D > P, L > U)	82	Neuro	RVs, neurogenic changes	R155C	DPD↑	Mental disorder, cerebellar signs
3	F/47	45	Myopathy	Brother (muscle weakness)	Fall down frequently, weakness of arms	Four limbs (P > D, L = U); neck flexion	94	Myo/ Neuro	RVs, neurogenic changes	R155C	No	No
4	M/51	38	LGMD	Father (muscle wasting, cramps)	Back pain	Paraspinal, four limbs (P > D, L > U)	490	Myo/ Neuro	RVs, neurogenic changes	R155H	No	No
5	M/44	32	DMRV	Father (SMA)	Numbness of left arm	Generalized, SW	44	Neuro	RVs, neurogenic changes	R191Q	No	No
6	M/43	39	DMRV	Father (MND) Sister (P7)	Atrophy of left shoulder girdle muscles	Four limbs (D > P, L > U), SW	215	Myo/ Neuro	RVs, neurogenic changes	A439P[a]	No	No
7	F/49	46	Myopathy	Father (MND) Brother (P6)	Weakness of lower limbs	Generalized	88	Neuro	RVs, neurogenic changes	A439P[a]	Osteo-sclerosis	Mental: borderline

F, female; M, male; D, distal; P, proximal; U, upper limb; L, lower limb; SW, scapular winging; Myo, myogenic changes; Neuro, vacuoles; CK, creatine kinase; EMG, electromyogram; DPD, deoxypyridinoline; VCP, valosin-containing protein; ND, not done; IBMPFD, inclusion body myopathy with Paget's disease of bone and frontotemporal dementia; LGMD; limb-girdle muscular dystrophy; DMRV, distal myopathy with rimmed vacuoles/hereditary inclusion body myopathy. [a]Novel mutation.

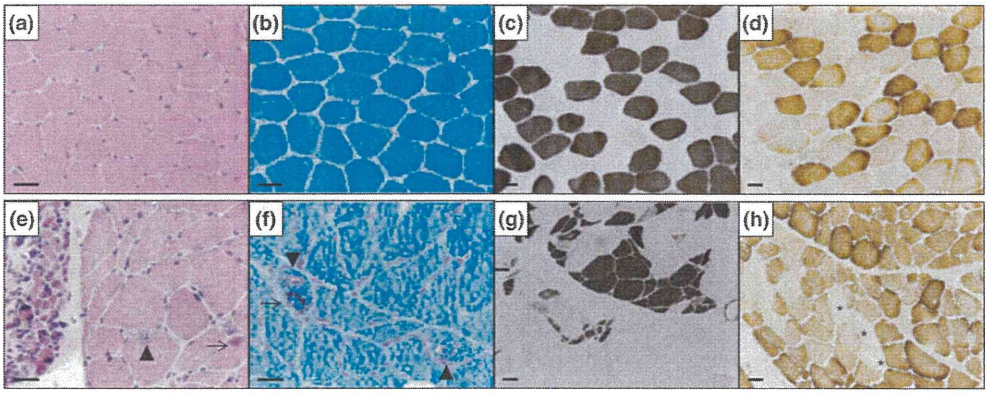

Figure 2 Histological analyses of muscle. (a–d: control. e–h: Patients 2 or 3. a and e: Hematoxylin and eosin (HE). b and f: modified Gomori trichrome (mGt). c and g: ATPase (pH 10.6). d and h: cytochrome *c* oxidase (COX). (e) HE staining of Patient 2 showed a group of atrophic fibers together with rimmed vacuoles (arrowheads) and a cytoplasmic inclusion (arrow). (f) A mGt stain of Patient 3 revealed rimmed vacuoles (arrowheads) and cytoplasmic bodies (arrow). (c) An ATPase stain of Patient 2 revealed grouped atrophy of darkly stained type 2 fibers and a large group of brightly stained type 1 fibers. Presence of scattered intermediate-colored type 2C fibers suggests immature fibers or fiber type conversion. (d) COX staining, which reflects mitochondrial electron transport enzyme activity, of Patient 3 showed some COX-deficient fibers (*). Bar = 50 μm.

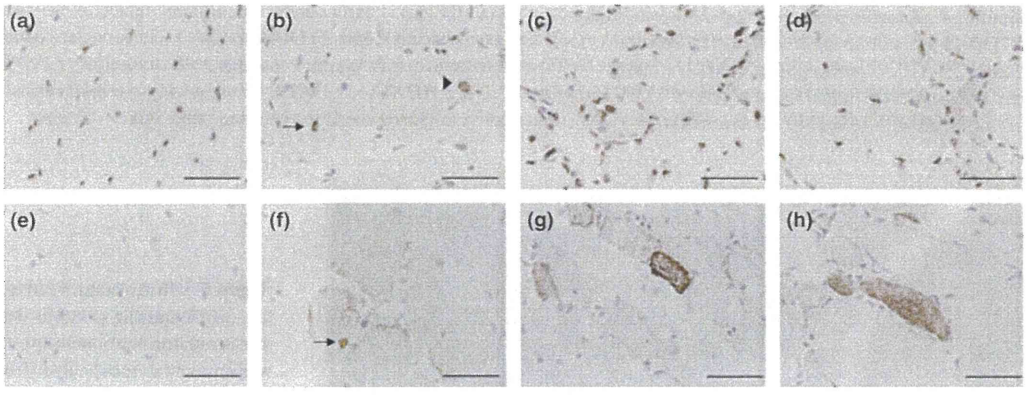

Figure 3 Immunostaining of transactivation response DNA-binding protein 43 (TDP-43) and valosin-containing protein (VCP). (a–d: TDP-43, e–h; VCP) In control muscle, clear nuclear staining of TDP-43 is seen (a), whereas VCP staining is barely detectable (e). In Patient 4, many nuclei show deficient TDP-43 staining, but scattered, strongly stained nuclei (arrow) and cytoplasmic aggregate (arrowhead) can be seen (b). VCP staining is seen in an enlarged nucleus (arrow) and subsarcolemma (f). In DMRV/hIBM (c) and sporadic inclusion body myositis (sIBM) (d) muscles, a smaller number of nuclei showing reduced staining of TDP-43 associated with cytoplasmic aggregations are seen. Some atrophic fibers show diffuse increased cytoplasmic staining of VCP in both distal myopathy with rimmed vacuoles/hereditary inclusion body myopathy (DMRV/hIBM) (g) and IBM (h). Bar = 50 μm.

VCP-positive cytoplasmic inclusions were seen, whereas no such inclusions were seen in control muscles (data not shown). Fibers with diffuse cytoplasmic staining of VCP were also seen in the patients with *VCP* mutations, DMRV/hIBM, or sIBM (Figs 3f–h and 4i).

Ultrastructural observations

Electron microscopic observations of muscles from Patients 2 and 4 revealed many abnormally shaped nuclei with condensed or scanty irregular heterochromatin, even in those muscle fibers with well-preserved myofibril structures (Fig. 5a and c). Some degenerating nuclei were surrounded by variable-sized membranous structures (data not shown). Filamentous inclusions that were 15–20 nm in diameter were also seen in both nuclei (Fig. 5b) and subsarcolemma (Fig. 5d and e). Subsarcolemmal accumulations of mitochondria, the presence of enlarged mitochondria, and paracrystalline inclusions were prominent in some muscle fibers (Fig. 5f).

Discussion

The number of the clinical reports of IBMPFD/ALS patients with *VCP* mutations is increasing; however, a

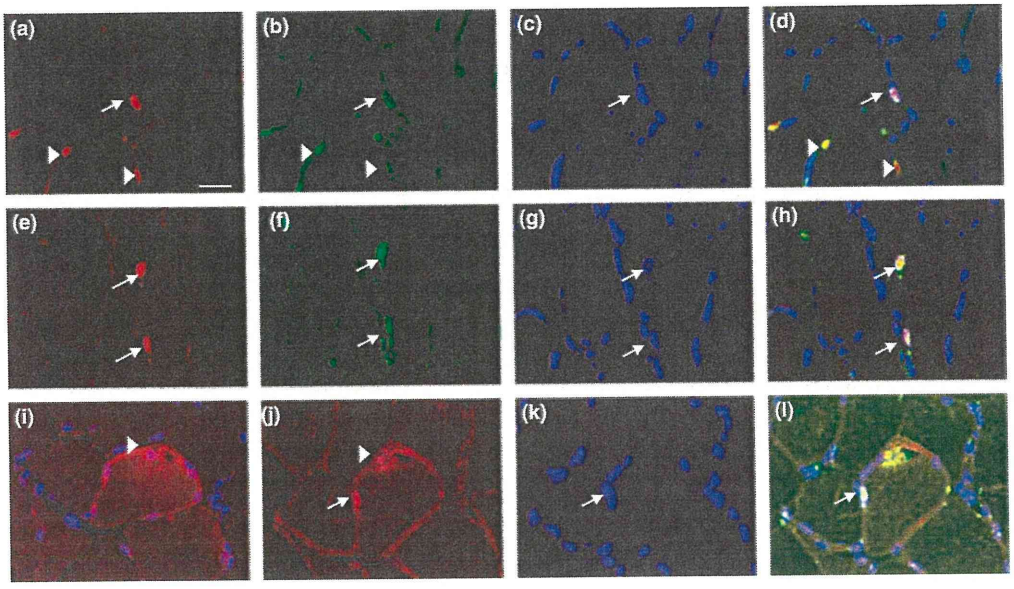

Figure 4 Immunohistochemical analyses of muscle. (a–d: a: TDP-43, b: ubiquitin, c: DAPI, d: merge) In the muscle from Patient 3, nuclear staining of transactivation response DNA-binding protein 43 (TDP-43) is barely detectable in many nuclei. Some strong positive signals of TDP-43 are seen in both nucleus (arrow) and cytoplasm (arrowheads). Most TDP-43-positive inclusions are costained with ubiquitin. (e–h: e: VCP, F: ubiquitin, g: DAPI, h: merge) VCP-positive nuclei (arrows) are costained with ubiquitin. (i) A VCP-positive muscle fiber with subsarcolemmal aggregation of VCP (arrowhead). (j–l: j: HDAC6, k: DAPI, l: merge with green-labeled ubiquitin) HDAC6 is costained with ubiquitin in nucleus (arrow) and subsarcolemma (arrowhead) in the same fiber. Bar = 25 μm.

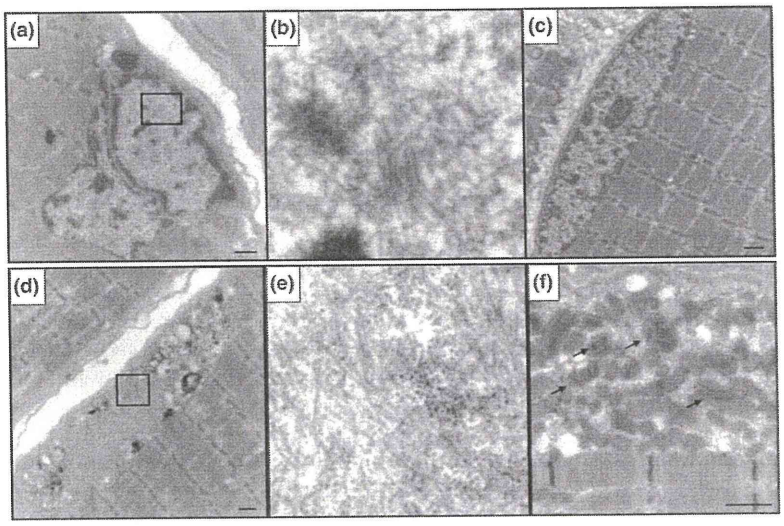

Figure 5 Ultrastructural analysis of muscle. (a) Myonuclei contains irregular heterochromatin with inclusion (square) in a well-preserved muscle fiber from Patient 2. (b) Magnified image of the region covered by the square in panel (a). A filamentous nuclear inclusion is seen. (c) A nucleus with well-preserved myofibrils in normal muscle. (d) A subsarcolemmal cytoplasmic inclusion containing filamentous structure. (e) Magnified image of the region covered by the square in panel (d). (f) A subsarcolemmal accumulation of enlarged mitochondria with paracrystalline inclusions (arrows) is seen in Patient 2. Bar = 1 μm.

Korean IBMPFD family is the only one to have been reported among Asian people [5]. Here, we show that VCP-related myopathy is not rare in an East Asian sample. Among 152 families with rimmed vacuolar myopathy, six families (4%) carried a heterozygous missense mutation including a novel p.Ala439Pro in exon 11. From the previous results that 39–64% of patients with *VCP* mutations have no rimmed vacuoles in their muscle biopsy [6,7], the incidence of VCP-opathy could be greater in myopathy patients. VCP is a member of ATPase associated with a variety of activities (AAA+) protein family and the alanine residue at position 439, located in the D1 ATPase domain, and is highly conserved among species. Furthermore, the p.Ala439Ser mutation was previously identified in a patient with IBMPFD [6].

In previous reports, more than half of the patients with *VCP* mutations have been reported to have PDB

[2]. Interestingly, only one of seven patients in our series showed a bone sclerotic region that was suggestive of PDB. PDB is reported to be rare in Asian populations and its frequency in Japan is 2.8 per 1 000 000 individuals, an incidence that is nearly 10 000 times less than that observed in Western countries [8]. The rare involvement of bone disease in Asian patients with *VCP* mutations might be related to ethnicity.

Frontotemporal dementia is another characteristic clinical symptom associated with *VCP* mutations and is observed in one-third of patients [2]. In our series, including elder affected relatives, mild mental disorder was noticed in only two patients. The cerebellar signs observed in Patient 2 are of note. Actually, the deceased elder brother of this patient had spinocerebellar degeneration. Although no patients with ataxia have been reported previously, we could not exclude the possibility of cerebellar involvement in this multisystem disorder.

Most of our patients and their symptomatic family members show isolated muscle involvement. Distribution of the affected muscles was variable, representing limb-girdle type, distal dominant, or scapuloperoneal type. Two patients showed asymmetrical involvement at the onset of the disease, which was also previously described in some IBMPFD patients [2,7,9]. Early involvement of the tibialis anterior muscles accompanied by rimmed vacuoles is indistinguishable from patients with DMRV/hIBM caused by *GNE* mutations [10]. Frequent involvement of the quadriceps femoris observed in patients with *VCP* mutations is important and helpful for differential diagnosis, because DMRV/hIBM is known as a quadriceps-sparing myopathy [11]. A combination of myogenic and neurogenic changes is an important and characteristic finding of VCP-related myopathy. Muscle cramps, pain, and fasciculation were often seen in our patients, which are also common findings in patients with motor neuron disease [12]. Pathological findings of grouped atrophy and fiber type grouping strongly suggest involvement of motor neurons and peripheral nerves. Electrophysiological results can support these findings. Like previous reports [6,8], the initial diagnosis of some affected family members in our series was motor neuron disease. The presence of these different diagnoses in the same family may be one of the characteristics of VCP-opathy.

Valosin-containing protein is involved in protein degradation by both the ubiquitin-proteasome system and the autophagic degradation system [13]. VCP is also reported to be involved in the maturation process during autophagosome formation [14]. Rimmed vacuoles, a common pathological change of VCP-related myopathy, are accumulations of membranous structures originating from autophagic vacuoles. Altered degradation of ubiquitinated proteins and autophagosome maturation may be closely associated with rimmed vacuolar formation. Consistent with this, ubiquitinated cytoplasmic and nuclear aggregations are another pathological hallmark of VCP-related myopathy. In this study, we demonstrate cytoplasmic and nuclear accumulations of ubiquitin, TDP-43, VCP, and also HDAC6. Accumulation of TDP-43 in the ubiquitinated inclusions is a characteristic pathological finding in brain and muscle from patients with *VCP* mutations as well as other neurodegenerative disorders including frontotemporal lobar degeneration with ubiquitin-positive inclusions and ALS without *VCP* mutations [15–17]. HDAC6, a cytoplasmic deacetylase, can transport ubiquitinated aggregates to the aggresome, the function of which is regulated by VCP [18]. HDAC6 is also known to involve maturation of autophagosomes [19]. Mutant VCP may influence the function of HDAC6, resulting in an accumulation of ubiquitinated proteins and insufficient protein degradation by autophagy.

Observations of electron microscopic images showed many abnormal nuclei, with or without filamentous inclusions that were seen in those muscle fibers with well-organized myofibril structures. This result suggests early nuclear damage as a key event of myopathy associated with *VCP* mutations. VCP is known to be involved in the maintenance and assembly of the nuclear envelope [20,21] and has been reported to have antiapoptotic effects [22]. Although the number of TUNEL-positive myonuclei in our samples was relatively small, mutant VCP can cause nuclear disorganization and dysfunction in skeletal muscle. Deficiency of nuclear localization of TDP-43 may also be closely associated with nuclear damage [23].

Prominent changes in mitochondria, including their localization, shape, deficiency in COX activity, and the presence of paracrystalline inclusions, strongly suggest mitochondrial dysfunction in VCP-related myopathy. Consistent with this, mutant VCP/cdc48 was reported to cause mitochondrial enlargement and dysfunction in yeast [24]. VCP has an important role in ubiquitin-dependent mitochondrial protein degradation, together with VCP/cdc48-associated mitochondrial stress-responsive 1 (Vms1) and Npl4 [25]. Further, abnormal cytoplasmic aggregations of TDP-43 are also known to cause mitochondrial damage and cell death [26,27]. Dysfunction of mitochondria in skeletal muscle could account for the muscle wasting observed in these patients.

Our study revealed clinical variability among Asian patients with *VCP* mutations. The rimmed vacuoles and ubiquitinated cytoplasmic aggregations, mixed myopathic and neuropathic changes, nuclear inclusions stained with VCP and HDAC6, and early nuclear and